

OECD MCCI Project
Small-Scale Water Ingression and Crust Strength Tests (SSWICS)
SSWICS-13 Test Data Report: Thermal Hydraulic Results

Rev. 1 - FINAL

April, 2010

by:

S. Lomperski, M. T. Farmer, D. Kilsdonk, R. Aeschlimann

Nuclear Engineering Division
Argonne National Laboratory
9700 S. Cass Avenue
Argonne, IL 60439
USA

Table of Contents

1. Introduction	1
1.1 Background	1
1.2 Summary Design Approach	2
2. System Description	2
2.1 General	2
2.2 Injection Supply System	6
2.3 Injection Nozzles	9
3. Data Acquisition and Control Systems	11
3.1 Instrumentation	11
3.2 General	12
4. Test Parameters and Course of Test	15
5. Sensor Malfunctions and Abnormalities	17
6. Data Reduction	20
7. Post Test Exams	21

List of Plots

A.1 Temperatures in tungsten thermowell; north melt quadrant	27
A.2 Temperatures in tungsten thermowell; south melt quadrant	27
A.3 Temperatures of selected steel structures	28
A.4 Total pressure in reaction vessel and position of selected valves	28
A.5 Condensate tank inventory as measured by ΔP and level sensors	29
A.6 Reservoir levels and condensate tank liquid inventory	29
A.7 HX secondary side flow rate, injection flow rate, and water injection valve position	30
A.8 Secondary side fluid temperatures at HX inlet and outlet	30
A.9 Miscellaneous gas and fluid temperatures	31
A.10 Fluid temperatures in the condensate tank	31
A.13 Sparge gas (N_2) flow rates	32
A.14 Heat flux as measured through condensate tank levels and HX heat load	32

1. Introduction

1.1 Background

Ex-vessel debris coolability is an important light water reactor (LWR) safety issue. For existing plants, resolution of this issue will confirm the technical basis for severe accident management guidelines (SAMGs). For new reactors, understanding this issue will help confirm the effectiveness of the design and implementation of new accident mitigation features and severe accident management design alternatives (SAMDAs). The first OECD-MCCI program conducted reactor material experiments focused on achieving the following technical objectives: i) provide confirmatory evidence and data for various cooling mechanisms through separate effect tests for severe accident model development, and ii) provide long-term 2-D core-concrete interaction data for code assessment and improvement.

Debris cooling mechanisms investigated as part of the first MCCI program included: i) water ingress through cracks/fissures in the core debris, ii) melt eruption caused by gas sparging, and iii) large-scale crust mechanical failure leading to renewed bulk cooling. The results of this testing and associated analysis provided an envelope (principally determined by melt depth) for debris coolability. However, this envelope does not encompass the full range of potential melt depths for all plant accident sequences. Cooling augmentation by additional means may be needed at the late stage to assure coolability for new reactor designs as well as for various accident sequences for existing reactors. In addition, the results of the CCI tests showed that lateral/axial power split is a function of concrete type. However, the first program produced limited data sets for code assessment. In light of significant differences in ablation behavior for different concrete types, additional data will be useful in reducing uncertainties and gaining confidence in code predictions.

Based on these findings, a broad workscope was defined for the follow-on MCCI program. The workscope can be divided into the following four categories:

1. Combined effect tests to investigate the interplay of different cooling mechanisms, and to provide data for model development and code assessment purposes.
2. Tests to investigate new design features to enhance coolability, applicable particularly to new reactor designs.
3. Tests to generate two-dimensional core-concrete interaction data.
4. Integral tests to validate severe accident codes.

In addition to the experimental work, an analysis task was defined to develop and validate coolability models to form the basis for extrapolating the experiment findings to plant conditions.

As one of the steps required to satisfy these objectives, the Management Board (MB) has approved the conduct of a third Category 2 Test to supplement the two that have already been approved. In particular, the following PRG recommendation was approved at the 5th PRG meeting:

Regarding the Category 2 small scale tests, PRG recommends that a SSWICS-13 test be performed with the bottom injection system partitioned into 2 parts, one with water only, the other with water and nitrogen. The test design report was prepared by the OA with input from KAERI. This report describes the test results for the third Category 2 test, which is denoted SSWICS-13.

1.2 Summary Design Approach

KAERI envisioned SSWICS-13 as a companion test to COMET-U2, which was performed for Forschungszentrum Karlsruhe (FZK) in 1997. It involved water injection through nine nozzles cast into a concrete basemat with the top of the nozzles positioned 15 mm below the surface of the concrete. The melt consisted of 50% UO_2 , 18% ZrO_2 , and 23 % borosilicate glass with the balance in chromium. The initial melt mass, depth, and temperature were 150 kg, 41 cm, and 2320 K, respectively. The melt was cooled to the solidus temperature within ~15 minutes of the onset of water injection and completely quenched after another ~22 minutes.

SSWICS-13 differs from COMET-U2 in that it is partitioned into two regions by tungsten plates in a fashion similar to that of SSWICS-12, which was partitioned into four regions. In addition, there are four nozzles rather than nine and the melt depth is 30 cm rather than 40 cm. The main test parameters for SSWICS-12, -13, and COMET-U2 are provided in Table 1.1 for reference.

For SSWICS-13, each nozzle is supplied by a dedicated reservoir so that water level changes can be used to determine flow rates. The two nozzles on one side of the partition include a capillary to supplement water injection with a stream of nitrogen gas. The apparatus is therefore configured to provide, in effect, two independent and simultaneous injection tests: one with a water/nitrogen mixture and a second only with water. The test data will be used to evaluate the effects of gas injection on the corium cooling rate and crust morphology. Ideally, the COMET-U2 melt depth and water injection rate would be replicated in SSWICS-13 to facilitate a comparison with the previous data. Unfortunately, the SSWICS operating envelop is unable to accommodate the COMET-U2 melt depth and condenser heat load. The remainder of this report describes the test apparatus, instrumentation, test procedure, data reduction, and test results.

2. System Description

2.1 General

The SSWICS reaction vessel (RV) has been designed to hold at least 100 kg of melt at an initial temperature of 2500°C. The RV lower plenum consists of a 67 cm long, 46 cm outer diameter carbon steel pipe (Fig. 2.1). The pipe is insulated from the melt by a 6.4 cm thick annulus of cast MgO that is denoted the “liner”. The selected pipe and insulation dimensions result in a melt diameter of 30 cm and a surface area of 707 cm². The melt depth for a typical corium charge of 75 kg is about 15 cm. This particular test used a 136 kg charge to create a 30 cm deep melt. The RV lower flange is insulated with a “basemat” consisting of 38 mm cast MgO covered by 25 mm of concrete. The basemat and liner form the crucible that holds the corium.

The RV upper plenum consists of a second section of pipe with a stainless steel protective liner. Three 10 cm pipes welded near the top of the vessel provide 1) a vent line for the initial surge of hot noncondensable gases generated by the thermite reaction, 2) a pressure relief line with a rupture disk (7.7 bar at 100°C), and 3) an instrument flange for the absolute pressure transmitter that measures the reaction vessel pressure. A baffle is mounted below the upper flange prevents water droplets from being carried up towards the condenser, which would adversely affect the heat flux measurement. A fourth 10 cm pipe welded to the top flange provides an outlet to carry steam from the quenching melt to four cooling coils. The water-cooled coils condense the steam, which is collected within a 200 cm high, 20 cm diameter condensate tank (CT). Fig. 2.2 gives an overview of the entire SSWICS melt-quench facility.

Table 1.1. Selected test parameters for SSWICS-12, -13, and COMET-U2.

Parameter	SSWICS-12	SSWICS-13	COMET-U2
Molten Corium Property	100 % oxidized PWR with 15 wt % siliceous concrete UO ₂ 55.61, ZrO ₂ 22.84, SiO ₂ 11.03, MgO 0.11, Al ₂ O ₃ 0.63, CaO 2.18, Cr 7.60%	100 % oxidized PWR with 15 wt % siliceous concrete UO ₂ 55.61, ZrO ₂ 22.84, SiO ₂ 11.03, MgO 0.11, Al ₂ O ₃ 0.63, CaO 2.18, Cr 7.60%	100 % oxidized PWR with 23 wt % borosilicate glass UO ₂ 49.92, ZrO ₂ 17.95, SiO ₂ 13.37, MgO 0.73, Al ₂ O ₃ 1.11, CaO 4.44, Cr 11.21, B ₂ O ₃ 1.27%
Test section diameter	30 cm	30 cm	30 cm
Initial melt mass	136 kg	136 kg	150 kg
Initial melt depth	30 cm	30 cm	40 cm
Initial melt temp.	2100 °C	2000 °C	2050 °C
Corium density	6000 kg/m ³	6000 kg/m ³	5120 kg/m ³
Specific heat	700 J/kg-K	700 J/kg-K	870 J/kg-K (2220-373K)
Basemat nozzles	4ea (same radius = 108mm)	2ea water 2ea water/gas (same radius = 106mm)	3×3 array (80mm pitch)
Nozzle diameter	32 mm	13.2 mm	13.2 mm
Nozzle characteristics	Porous concrete	Single tube for water Double tube for water/gas	
Concrete thickness above nozzles	0 mm	10 mm	15 mm
Partition	4 regions	2 regions	None
Water supply pressure	0.2, 0.15, 0.1, 0.05bar	0.2 bar	0.2 bar
Max. water flow rate	~ 2.4 lpm	~ 1.2 lpm	~ 13 lpm
Max. gas flow rate	N.A.	0.24 lpm (20% of water flow rate)	N.A.
Basemat construction	Inert MgO	25 mm thick limestone/common sand concrete with underlying 38 mm thick inert MgO	Glass 75.8%, Type 1 Cement 15.2%, Water 9.0%
Quenching time	~ 60 min (to 100°C)	~ 150 min (to 100°C)	~ 35 min (<230 °C)

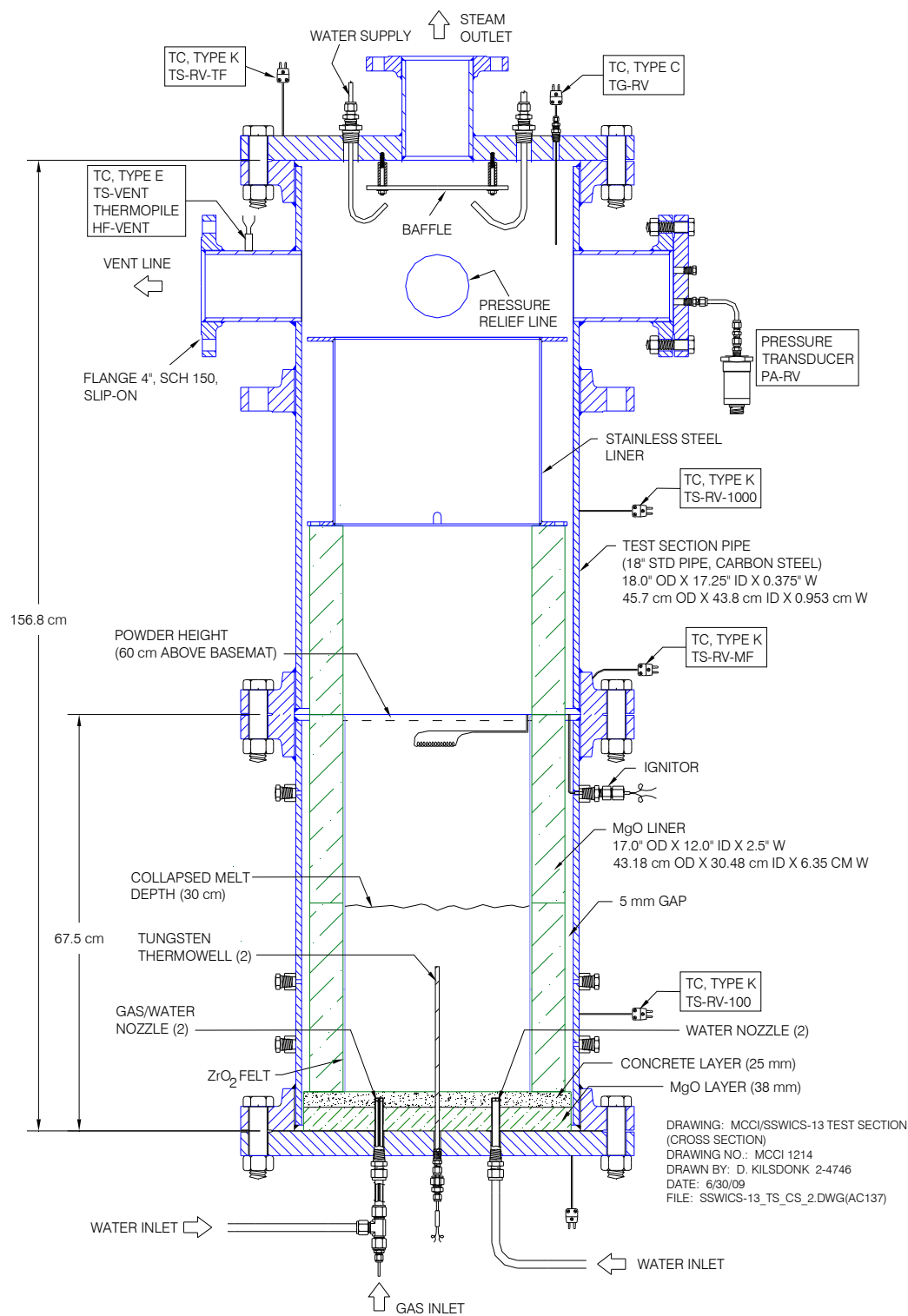


Figure 2.1. Side view of reaction vessel.

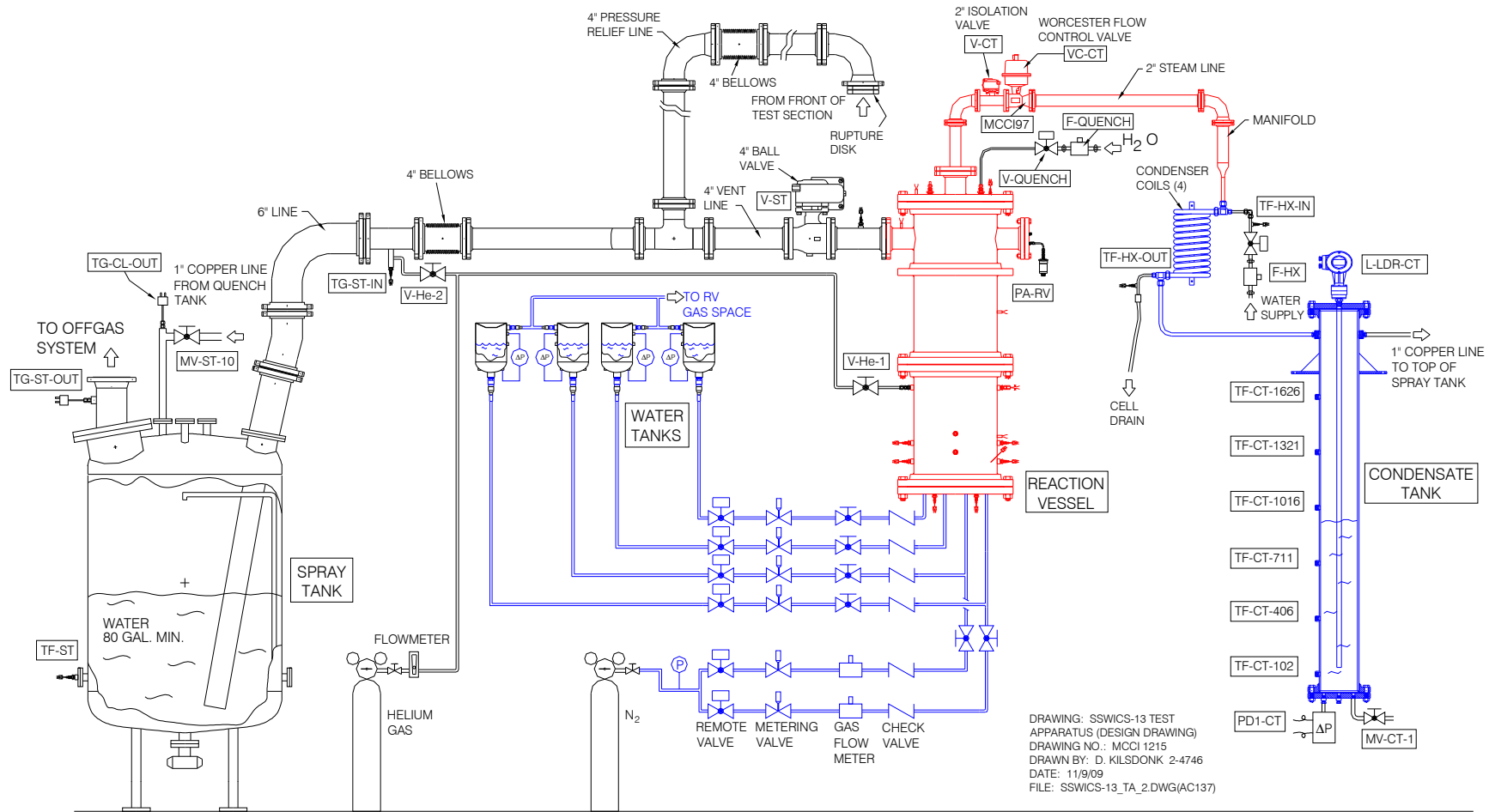


Figure 2.2. SSWICS melt quench facility.

Like SSWICS-12, the corium will be divided into sectors using metallic partitioning plates. As part of the planning process for SSWICS-12, it was concluded that tungsten was the best candidate material for this application since it has the highest strength of the refractory metals at high temperature, which minimizes the required thickness and, thereby, the heat sink provided by the partition. A plate thickness of 10 mm was selected for that test, and the same was recommended for this one. The test section is divided into two by a 60 cm-high wall made up of three 20 cm high plates. The partition is supported by grooves in the liner to discourage shifting under lateral loads. The basemat detail is shown in Fig. 2.3.

2.2 Injection Supply System

Each nozzle is served by a single supply tank so that a differential pressure transmitter can be used to measure the flow rate to individual nozzles. The nozzles are gravity fed so that the driving pressure for injection is set by the elevation difference between the nozzle and the tank water level (Fig. 2.4). A check valve in each line prevents back flow up into the tank. There is also an isolation valve in each line that is opened after the thermite burn is completed and the melt has contacted the basemat.

The tanks are positioned at identical levels to generate the same water head on each nozzle. A pressure equalization line links the RV gas space to the gas spaces of all four tanks, ensuring that the driving head for the nozzles is set only by the nozzle/tank elevation difference. This is necessary because the RV pressure spikes for a short period following initial water injection. If the reservoir gas plenums are not maintained at the same pressure as the RV plenum, the initial pressure spike will halt water injection, causing steam production and RV pressure to drop, which in turn permits continued water injection. It is likely that the system would oscillate during the early period of the test. Connecting the gas spaces of the reservoirs with that of the RV should prevent such oscillations.

Figure 2.4 shows the positioning of the tanks, which are set to provide a driving head of 0.2 bar. The net driving head ΔP is defined here as the head remaining after subtracting the hydrostatic head associated with the melt:

$$\Delta P = \rho_l g L - \rho g h \Big|_{\text{corium}}$$

where h is the height of the corium, 30 cm for this test, L is the distance from the bottom of the corium pool to the tank water surface, and ρ_l and ρ are the coolant and corium densities, respectively. The head associated with the corium was calculated to be 0.15 bar by assuming a density of 5120 kg/m^3 . Assuming a water head of 10 meters/ bar, the tanks are thus positioned 3.6 meters above the bottom of the corium pool.

In the interest of simplicity, no system is used to replenish the tanks during the test to maintain water level and so the driving head falls as water is injected into the melt. The drop in water level can be made small by using large-diameter tanks, but they serve as pressure vessels and so there is a strong incentive to minimize their size. The initial water inventory for each tank is 15 liters, which was chosen by noting that approximately 30 liters of water is collected by the condensate tank during a typical 75 kg test. Since this test involves 136 kg of corium and a higher than normal initial temperature, it was expected that about 60 liters of water would be boiled off while quenching the melt.

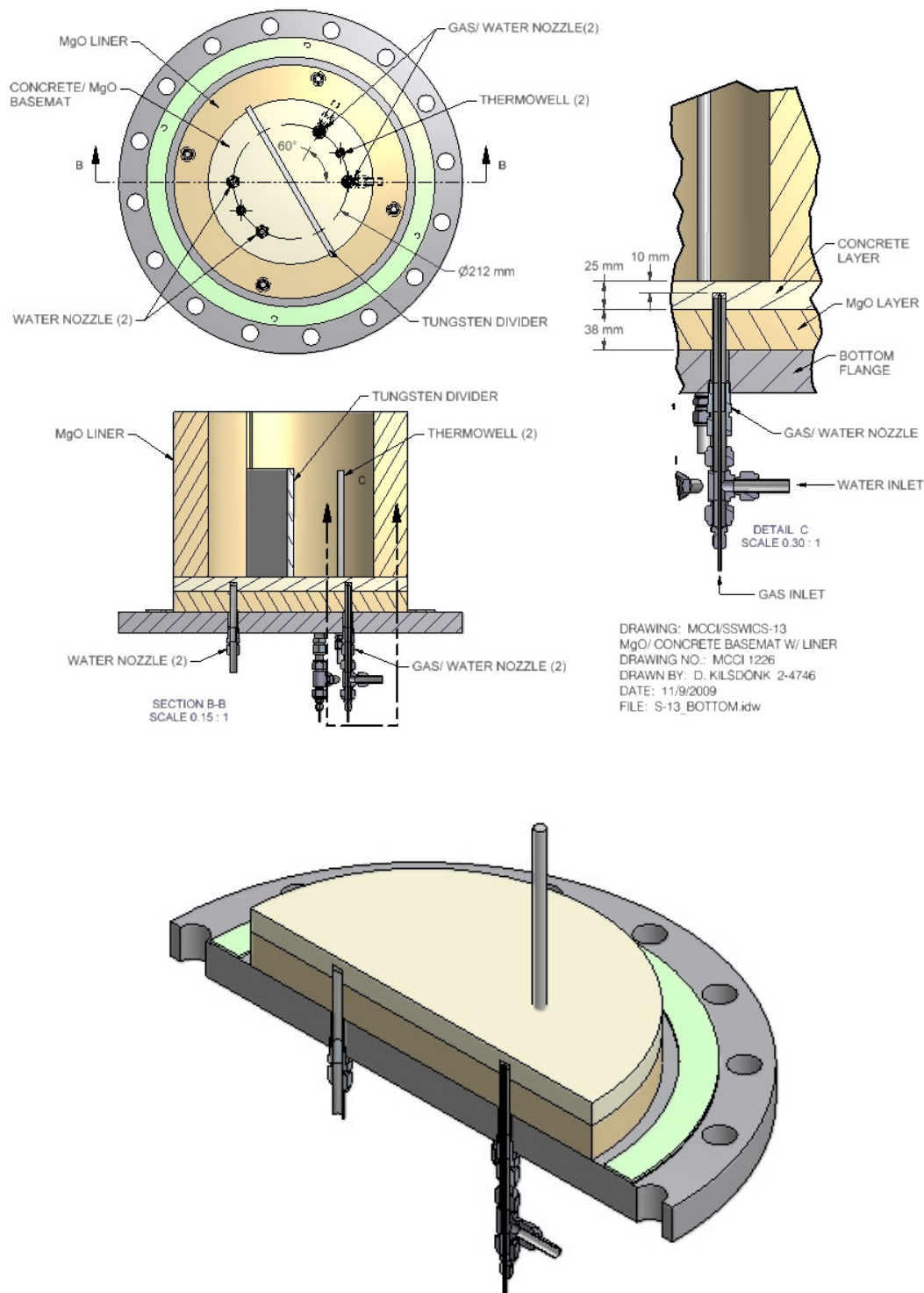


Figure 2.3. Lower plenum and basemat detail.

The PRG had recommended supplementary water injection from the top shortly after water flow from below is established. The purpose is to cool the superheated steam generated in the very early stages of the test. During the first minutes of SSWICS-12, a peak upper plenum temperature of 1700°C was measured, which is excessive for the steel vessel. Twenty liters were to be injected from above as soon as bottom injection was confirmed.

During the early stage of the experiment, it is likely that the water injected into the melt is completely vaporized. It is therefore necessary to limit the injection flow rate so that the condensing system is not overwhelmed. The condensing system has a capacity of approximately 0.08 kg/s. The flow limit for SSWICS-12 was set at 50% this capacity. The condensing system proved adequate for those conditions, but melt was ejected from the lower plenum and left a coating over most of the inside of the RV. In hopes of avoiding melt ejection in this test, the flow rate limit was cut in half to 0.005 kg/s per nozzle. At this maximum flow rate of 0.02 kg/s into the melt, complete vaporization would dissipate 45 kW, or 600 kW/m².

Nozzle permeability is high enough that a restriction on the injection line is required to prevent the flow rate from exceeding the specified limit. Each line has a metering valve set to allow 0.005 kg/s at the initial fill level, which would empty the tanks in ~50 minutes if this maximum rate is maintained.

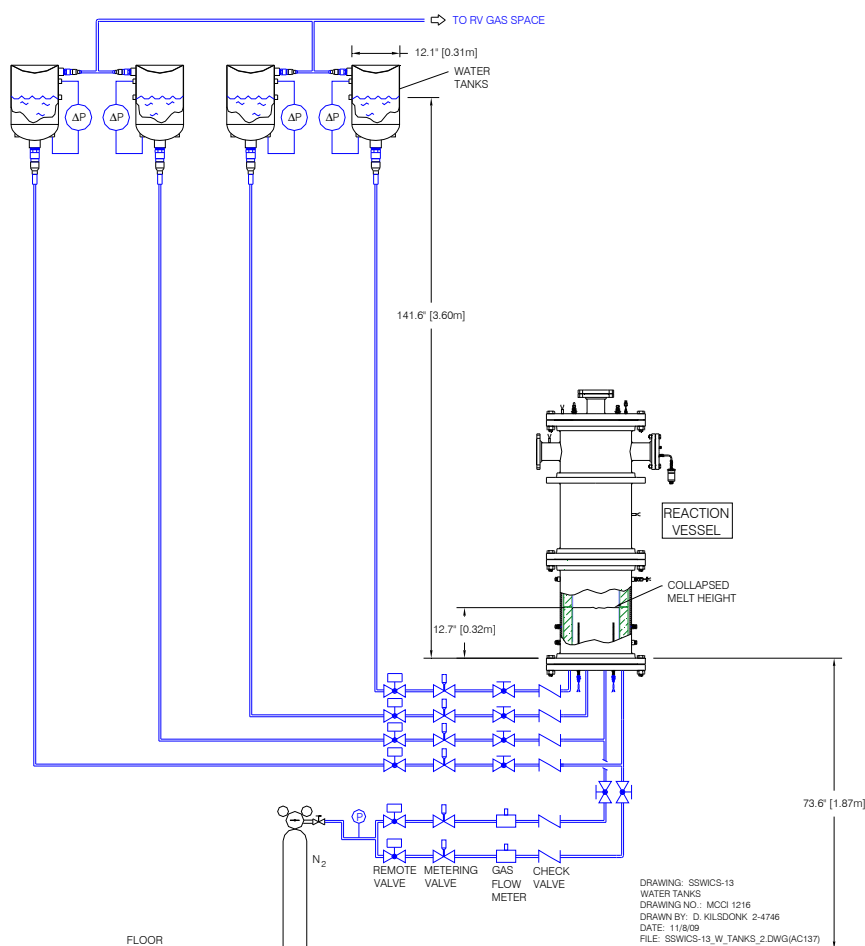


Figure 2.4. Water injection system geometry (drawn to scale).

2.3 Injection Nozzles

The design of the nozzles is illustrated in Fig. 2.5. Water leaves the nozzle and enters the melt through four 1 mm-diameter holes. The holes are positioned 4.5 mm from the nozzle center. The nozzle itself has a diameter of 12 mm and all components are made of stainless steel. The two nozzles injecting nitrogen have an additional 1-mm hole at the center. The nitrogen and water are expected to mix together as they enter the melt and it is thought that the noncondensable gas will reduce the likelihood of vapor explosions.

KAERI has specified the flow rate of the gas to be 20% the initial volumetric flow rate of the water. It was originally planned to deliver the gas using a flow controller set at a constant flow rate. However, there was concern that the forced gas flow might suppress the natural circulation water flow since the two are combined beneath a heavy corium pool. There is also concern that the combination of forced and natural circulation flow will not generate good gas/water mixing near the nozzle. To address these concerns, we switched to a pressure regulated flow.

The gas system (Fig. 2.6) was configured with an approach similar to that used for the water. The initial flow rate to each nozzle is defined (0.06 lpm), as is the maximum driving pressure at the nozzle exit (0.2 bar to match the initial net driving head set for the water). The head associated with the corium is 0.15 bar and so the gas source pressure is set at 0.35 bar to provide the net 0.2 bar driving pressure.

The metering valve is used to adjust the line losses to achieve the target flow rate. Since the corium is not present beforehand to contribute to the net head, the adjustment must be made without it. The capillary was removed from the fitting at the Swagelok tee shown in the figure. With the source pressure at 0.35 bar, the pressure drop between the source and the end of the gas line is 0.35 bar rather than the 0.2 bar expected during the test. The correct valve position was determined by considering the relationship between flow and pressure drop:

$$\dot{V} = N C_v \Delta P^{1/2}$$

Where \dot{V} is the volumetric flow rate, N is a constant, C_v the metering valve loss coefficient, and ΔP the pressure drop across the valve. Most of the pressure drop between the source and nozzle occurs across the metering valve. The required C_v (valve position) for 0.06 lpm at 0.2 bar ΔP is found by using the above equation twice along with the 0.35 bar used to adjust the metering valve:

$$\frac{0.06}{x} = \left(\frac{0.2}{0.35} \right)^{1/2} \quad x = 0.079 \text{ lpm}$$

Thus the metering valve position that will provide 0.06 lpm at a ΔP of 0.2 bar will give 0.079 lpm at 0.35 bar. The metering valves were adjusted until the flow meters showed 0.079 lpm. The isolation valves were then closed and the tubing was reattached to the Swagelok tee.

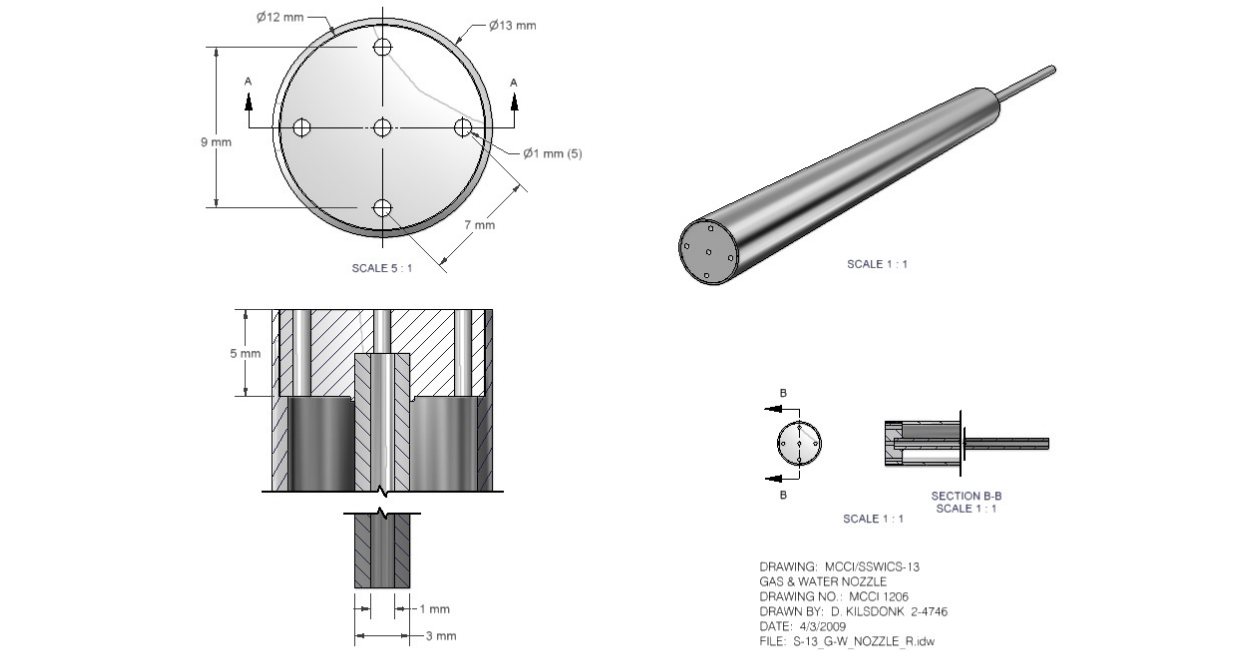


Figure 2.5. Gas/water nozzle construction detail.

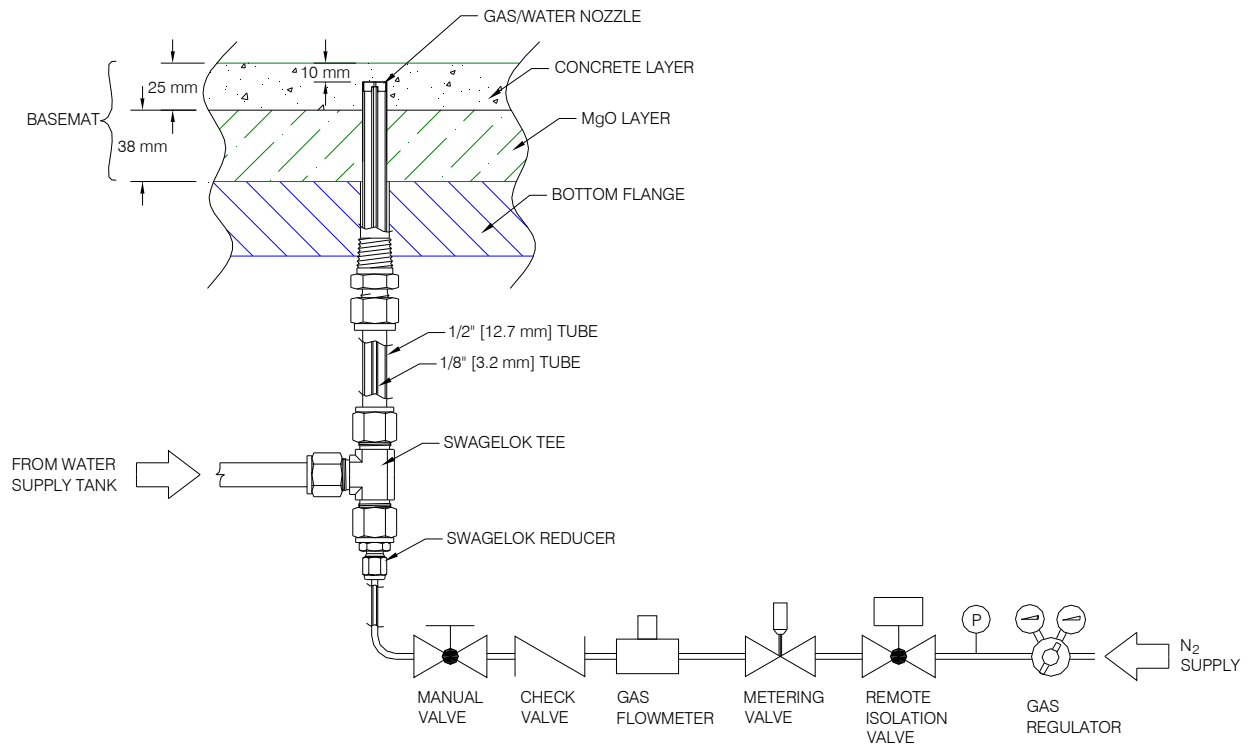


Figure 2.6. Injection system configuration.

3. Data Acquisition and Control Systems

3.1 Instrumentation

This test is intended to determine the efficacy of a particular engineered melt cooling concept. The directive to test a partitioned melt with separate injectors is, in effect, an instruction to combine two quench experiments into one. The instrumentation must therefore provide data sufficient to determine the boundary conditions and cooling behavior of the two partitions. The flow rate and driving pressure of each nozzle will be measured along with melt temperatures. The nitrogen gas flow rates to the two nozzles will also be measured. The condensate collection and measurement system used in past tests to determine the steaming rate will also be used in this test, but it cannot provide the cooling rate of a particular partition. It will instead provide the gross melt cooling rate. Only indirect indications of individual partition cooling rates, obtained through measurements of melt temperature and water flow rate into each quadrant, are available for this test.

Figure 3.1 shows the thermocouple layout in the basemat and the liner. Each partition is allotted one 5-junction C-type thermocouple assembly in a tungsten thermowell. The thermocouples are spaced every 51 mm so that the uppermost thermocouple is 195 mm above the basemat surface. The tungsten thermowells are 9.5 mm diameter, which is the same size used in CCI tests but larger than that used in previous SSWICS tests (6 mm). Though thermowell size should be minimized to limit fin cooling effects, the thermowells for this test are too long to fabricate in a diameter less than 9.5 mm.

MgO liner thermocouples used in previous tests to detect water bypass around the melt at the melt/liner interface are omitted as they were in SSWICS-12. These measurements are irrelevant here as water injection is expected to create widespread melt porosity that should indeed allow liquid flow across

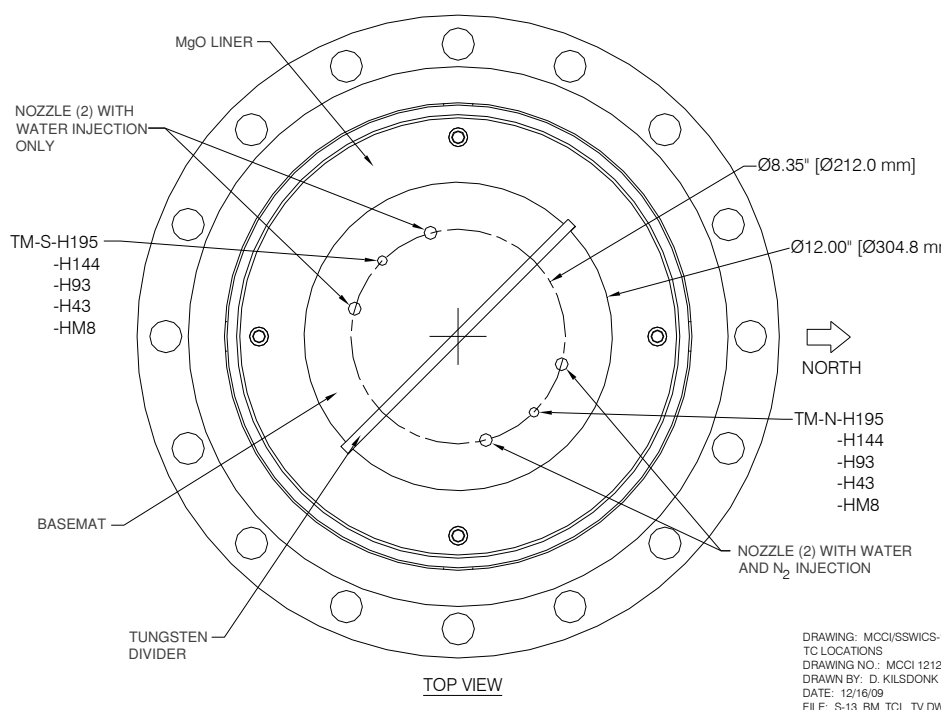


Figure 3.1. Melt thermocouple locations.

the melt/liner interface. Thus there is no notion here that water could go “around” the melt, as it might have during previous water ingression tests, distorting the predominantly one-dimensional character of the quench front.

The nomenclature used to identify thermocouples is as follows: TM (temperature within the corium melt), TF (fluid temperature), TG (gas space temperature), TS (structure temperature), H# (height above the bottom of the melt, in mm, and N, S, E, W representing the cardinal points. The partition is to be situated so that the “wedges” face towards the cardinal points. For example, TM-N-H195 is the melt thermocouple in the north facing wedge, 195 mm above the bottom of the melt. An instrument list is provided in Table 3.1.

3.2 General

All data acquisition and process control tasks are managed by a PC executing LabVIEW 8.2 under Windows XP. Sensor output terminals are connected to model HP E1345A 16-channel multiplexers and the signals are digitized by an HP E1326B 5 ½ digit multimeter located within the test cell (Fig. 3.2). Signal noise is reduced by integration over a single power line cycle (16.7 ms). The digitized sensor readings are routed from the test cell to the PC in the control room via two HP-IB extenders. The extenders allow the ASCII data from the HP to be sent through the cell wall over a BNC cable. The

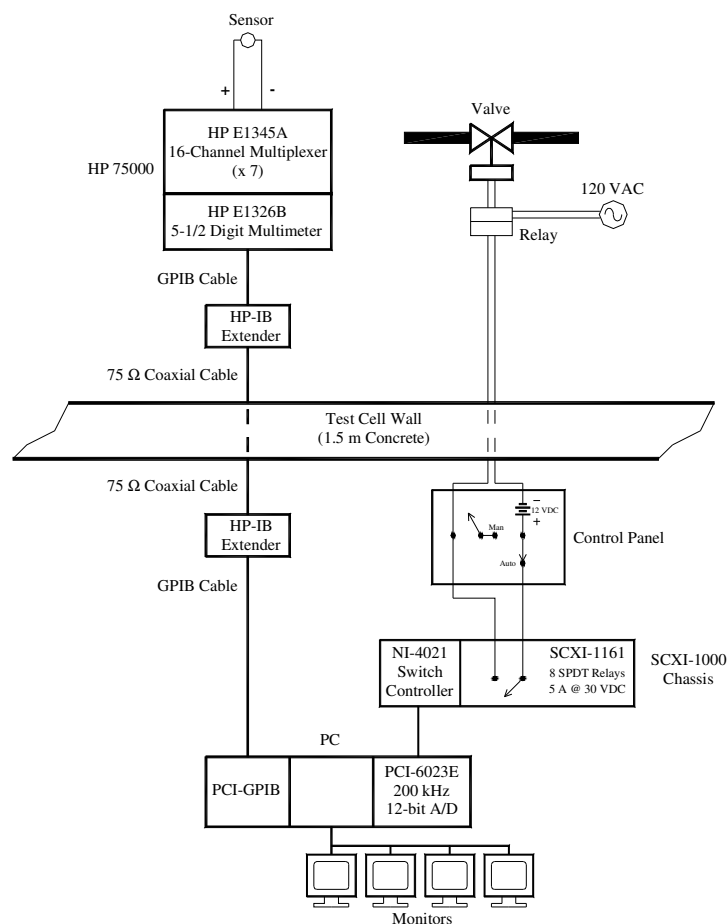


Figure 3.2. Data acquisition and control systems.

#	Channel	Name	Type	Description	Serial #	Output	Range	Accuracy
0	HPS-0	T-CJ-HPS	AD5921C	Cold junction compensation sensor.	-	1□A/K	0-70°C	±0.5°C
1	HPS-1	TM-N-H195	TC type C	Melt temp. 195 mm above bottom of melt (in tungsten thermowell).	-	0-37 mV	0-2320°C	±4.5°C or 1%
2	HPS-2	TM-N-H144	TC type C	Melt temp. 144 mm above bottom of melt (in tungsten thermowell).	-	0-37 mV	0-2320°C	±4.5°C or 1%
3	HPS-3	TM-N-H93	TC type C	Melt temp. 93 mm above bottom of melt (in tungsten thermowell).	-	0-37 mV	0-2320°C	±4.5°C or 1%
4	HPS-4	TM-N-H42	TC type C	Melt temp. 43 mm above bottom of melt (in tungsten thermowell).	-	0-37 mV	0-2320°C	±4.5°C or 1%
5	HPS-5	TM-N-Hm9	TC type C	Melt temp. 8 mm below bottom of melt (in tungsten thermowell).	-	0-37 mV	0-2320°C	±4.5°C or 1%
6	HPS-6	TM-S-H195	TC type C	Melt temp. 195 mm above bottom of melt (in tungsten thermowell).	-	0-37 mV	0-2320°C	±4.5°C or 1%
7	HPS-7	TM-S-H144	TC type C	Melt temp. 144 mm above bottom of melt (in tungsten thermowell).	-	0-37 mV	0-2320°C	±4.5°C or 1%
8	HPS-8	TM-S-H93	TC type C	Melt temp. 93 mm above bottom of melt (in tungsten thermowell).	-	0-37 mV	0-2320°C	±4.5°C or 1%
9	HPS-9	TM-S-H42	TC type C	Melt temp. 43 mm above bottom of melt (in tungsten thermowell).	-	0-37 mV	0-2320°C	±4.5°C or 1%
10	HPS-10	TM-S-Hm9	TC type C	Melt temp. 8 mm below bottom of melt (in tungsten thermowell).	-	0-37 mV	0-2320°C	±4.5°C or 1%
11	HPS-11	Reserve	-	-	-	-	-	-
12	HPS-12	Reserve	-	-	-	-	-	-
13	HPS-13	Reserve	-	-	-	-	-	-
14	HPS-14	Reserve	-	-	-	-	-	-
15	HPS-15	Reserve	-	-	-	-	-	-
16	HPS-16	Reserve	-	-	-	-	-	-
17	HPS-17	Reserve	-	-	-	-	-	-
18	HPS-18	Reserve	-	-	-	-	-	-
19	HPS-19	Reserve	-	-	-	-	-	-
20	HPS-20	TF-quench	TC type K	Temperature of water injected into RV	-	0-50 mV	0-1250°C	±2.2°C or 0.75%
21	HPS-21	TG-RV	TC type C	Gas temp. in reaction vessel upper plenum.	-	0-37 mV	0-2320°C	±4.5°C or 1%
22	HPS-22	TS-RV-tf	TC type K	Temperature of RV top flange.	-	0-50 mV	0-1250°C	±2.2°C or 0.75%
23	HPS-23	TS-RV-1000	TC type K	Outer wall temp. of RV 1000 mm above bottom of melt.	-	0-50 mV	0-1250°C	±2.2°C or 0.75%
24	HPS-24	TS-RV-mf	TC type K	Temperature of RV middle flange.	-	0-50 mV	0-1250°C	±2.2°C or 0.75%
25	HPS-25	TS-RV-100	TC type K	Outer wall temp. of RV 100 mm above bottom of melt.	-	0-50 mV	0-1250°C	±2.2°C or 0.75%
26	HPS-26	TS-RV-bf	TC type K	Temperature of RV bottom flange.	-	0-50 mV	0-1250°C	±2.2°C or 0.75%
27	HPS-27	Reserve	-	-	-	-	-	-
28	HPS-28	TF-CT-102	TC type K	Fluid temp. in condensate tank at a water level of 102 mm.	-	0-50 mV	0-1250°C	±2.2°C or 0.75%
29	HPS-29	TF-CT-406	TC type K	Fluid temp. in condensate tank at a water level of 406 mm.	-	0-50 mV	0-1250°C	±2.2°C or 0.75%
30	HPS-30	TF-CT-711	TC type K	Fluid temp. in condensate tank at a water level of 711 mm.	-	0-50 mV	0-1250°C	±2.2°C or 0.75%
31	HPS-31	TF-CT-1016	TC type K	Fluid temp. in condensate tank at a water level of 1016 mm.	-	0-50 mV	0-1250°C	±2.2°C or 0.75%
32	HPS-32	TF-CT-1321	TC type K	Fluid temp. in condensate tank at a water level of 1321 mm.	-	0-50 mV	0-1250°C	±2.2°C or 0.75%
33	HPS-33	TF-CT-1626	TC type K	Fluid temp. in condensate tank at a water level of 1626 mm.	-	0-50 mV	0-1250°C	±2.2°C or 0.75%
34	HPS-34	TF-HX-in	TC type K	Fluid temp. at HX coolant inlet.	-	0-50 mV	0-1250°C	±2.2°C or 0.75%
35	HPS-35	TF-HX-out	TC type K	Fluid temp. at HX coolant outlet.	-	0-50 mV	0-1250°C	±2.2°C or 0.75%

Table 3.1. Instrumentation list for water ingress tests (part 1 of 2).

#	Channel	Name	Type	Description	Serial #	Output	Range	Accuracy
36	HPS-36	Reserve	-	-	-	-	-	-
37	HPS-37	I-ign	DC supply	Current supply for thermite ignitor.	-	0-100 mV	0-25 Amps	-
38	HPS-38	F-spargel	FMA1810	Flow rate of nitrogen into injector for gas sparging	243485-3	0 - 5 V	0-0.2 lpm N2	±0.003 lpm
39	HPS-39	F-spargel2	FMA1810	Flow rate of nitrogen into injector for gas sparging	243485-2	0 - 5 V	0-0.2 lpm N2	±0.003 lpm
40	HPS-40	PA-RV	1810AZ	Absolute pressure in reaction vessel.	02351-00P1PM	1-6 V	0-14 bar gage	±0.14 bar
41	HPS-41	PD-CT	1801DZ	∅ P transmitter to measure condensate inventory.	-	0-13 V	0-0.35 bar	±0.004 bar
42	HPS-42	L-TDR-CT	BM100A	Time domain reflectometer to measure CT level.	A02331879A	4 - 20 mA	0 - 2 m	±3 mm
43	HPS-43	VDC-P-supply	-	Voltage of the power supply for the pressure transmitters.	-	0 - 15 V	-	-
44	HPS-44	PD-R1	-	∅ P transmitter to measure level in reservoir.	D2	0-13 V	0-0.35 bar	±0.004 bar
45	HPS-45	PD-R2	-	∅ P transmitter to measure level in reservoir.	D5	0-13 V	0-0.35 bar	±0.004 bar
46	HPS-46	PD-R3	-	∅ P transmitter to measure level in reservoir.	D3	0-13 V	0-0.35 bar	±0.004 bar
47	HPS-47	PD-R4	-	∅ P transmitter to measure level in reservoir.	D4	0-13 V	0-0.35 bar	±0.004 bar
60	HPQ-50	T-CJ-HPQ	AD592 IC	Cold junction compensation sensor.	-	1∅ A/K	0-70°C	±0.5°C
61	HPQ-51	TF-ST	TC type K	Fluid temp. in spray tank.	-	0-50 mV	0-1250°C	±2.2°C or 0.75%
62	HPQ-52	TG-CL-out	TC type K	Gas temperature in condensate tank outlet line to spray tank.	-	0-50 mV	0-1250°C	±2.2°C or 0.75%
63	HPQ-53	TG-ST-in	TC type K	Gas temp. in the spray tank line inlet.	-	0-50 mV	0-1250°C	±2.2°C or 0.75%
64	HPQ-54	TG-ST-out	TC type K	Gas temp. in the spray tank line outlet.	-	0-50 mV	0-1250°C	±2.2°C or 0.75%
65	HPQ-55	F-quench	Paddlewheel	Flow rate of water into reaction vessel (for quenching melt).	3144	0-5 V	0-50 gpm	±0.5 gpm
66	HPQ-56	F-HX	Paddlewheel	Flow rate of cold water to heat exchangers.	3143	0-5 V	0-50 gpm	±0.5 gpm
67	HPQ-65	Reserve	-	-	-	-	-	-
68	HPQ-66	P-spargel	-	∅ P transmitter for spargel gas back pressure	-	0-13 V	0-2 bar	±0.02 bar
69	HPQ-67	Reserve	-	-	-	-	-	-

Table 3.1. (continued).

LabVIEW Channel #	Valve Name	Type	Description	Actuator
1	V-CT	Ball valve	Valve on steam line between reaction vessel and quench tank.	Pneumatic
2	V-quench	Ball valve	Valve on quench water supply line into reaction vessel.	Solenoid
3	V-quench-i	Ball valve	Isolation valve on quench water supply line into reaction vessel.	Solenoid
4	V-quench-b	Ball valve	Valve on back-up quench water supply.	Solenoid
5	V-ST	Ball valve	Valve on vent line between reaction vessel and spray tank.	Pneumatic
Panel	V-HX	Ball valve	Valve on cooling-water line to heat exchangers.	Solenoid
Panel	VC-CT	Ball valve	Control valve on steam line between reaction vessel and quench tank.	Electric
Panel	V-R1	Ball valve	Control valve on water injection line from reservoir R1.	Electric
Panel	V-R2	Ball valve	Control valve on water injection line from reservoir R2.	Electric
Panel	V-R3	Ball valve	Control valve on water injection line from reservoir R3.	Electric
Panel	V-R4	Ball valve	Control valve on water injection line from reservoir R4.	Electric
Panel	V-spargel	Ball valve	Control valve on sparge line one.	Electric
Panel	V-spargel2	Ball valve	Control valve on sparge line two.	Electric

Table 3.2. Remotely operated valves.

extender within the control room then communicates with a GPIB card within the PC. This configuration also permits remote control of the multimeter through LabVIEW. The power line cycle integration results in a minimum (theoretical) time of 0.75 s to scan the channel list (16.7 ms * 45 channels). In practice, however, the acquisition of a single scan is at a frequency of approximately 0.5 Hz.

Selected valves are controlled with the PC using a relay card housed within an SCXI chassis (National Instruments); see Table 3.2. These electromechanical relays are capable of switching up to 8 A at 125 VAC or 5 A at 30 VDC. They are operated via a switch controller in the SCXI chassis, which communicates with the PC through a general-purpose data acquisition card. As shown in Fig. 3.2, the relays in the control room operate devices within the test cell indirectly, through a second relay. This is intended to provide an additional level of electrical isolation between the NI switching hardware and high voltage sources within the cell. As an added safety measure, all wiring is routed through a control panel that can be switched from automatic (PC) control to manual control in the event of computer failure.

4. Test Parameters and Course of Test

The oxide phase of the corium composition for SSWICS-13 is the same as that of SSWICS-6 and SSWICS-12 (i.e., 60.3/24.7/15.0 wt % $\text{UO}_2/\text{ZrO}_2/\text{siliceous concrete}$). However, consistent with SSWICS-12, the thermite reacts at a higher temperature relative to SSWICS-6 to minimize crust formation on the basemat that might impair concrete erosion and the initiation of water flow through the nozzles. This thermite reacts at $\sim 2100^\circ\text{C}$ rather than $\sim 1950^\circ\text{C}$ for the SSWICS-6 formula. Reformulation of the thermite to produce the higher reaction temperature results in a slightly higher Cr metal byproduct content of 7.6 wt % in the melt, which can be compared with to the level of 6.4 wt % for the SSWICS-6 thermite. The corium constituents are listed in Tables 4.1 and test parameters for the entire SSWICS series are provided in Table 4.2.

Constituent	Mass (kg)
U ₃ O ₈	78.61
CrO ₃	19.90
CaO	2.96
Zr	22.98
Mg	0.10
Si	3.51
SiO ₂	7.49
Al	0.45
Total	136.0

Tables 4.1. . Corium powder charge and reaction product mass fractions.

Constituent	Wt %	
	Reactant	Product
U ₃ O ₈	57.80	-
UO ₂	-	55.61
Zr	16.90	-
ZrO ₂	-	22.84
Si	2.58	-
SiO ₂	5.51	11.03
Mg	0.07	-
MgO	-	0.11
Al	0.33	-
Al ₂ O ₃	-	0.63
CaO	2.18	2.18
CrO ₃	14.63	-
Cr	-	7.60

The metering valves on the water lines were adjusted so that each tank would provide an initial flow rate of 0.005 kg/s. The adjustments were made over several fill and drain runs. The day of the test, the tanks were each filled with water to a level of ~0.3 m to provide the initial net driving heads of 0.2 bar. The source pressure for the nitrogen sparging lines was set to 0.35 bar and the metering valves adjusted until the flow to each meter showed 0.079 lpm (section 2.3).

The test proceeded as follows:

- 1) RV structures were preheated to ~100°C.
- 2) The water for top injection was preheated to ~100°C.
- 3) The thermite ignition system was armed and the door to the cell closed.
- 4) The thermite was ignited to initiate the test.
- 5) First temperature increase noted in TG-RV (defined in plots as t=0)
- 6) Peak melt temperatures of ~2000°C were reached in the north and south sections at t=70 and 80 s, respectively.
- 7) At 60 s the valve on the steam line to the condensate tank was opened and at 82 s the signal to close the surge tank valve was sent so that steam would be routed to the condenser and condensate tank. The surge tank valve takes 10-15 s to fully close.
- 8) When closure of the surge tank valve was confirmed, the isolation valves on the water and sparge lines were opened (no signals available for the DAS).
- 9) The first rise in the HX outlet temperature was detected at 70 s while the first increase in the TDR level occurred at roughly 150 s.
- 10) Gas injection begins from both lines at 74 s.
- 11) Reservoir level measurements are noisy, but by roughly 300 s it is clear that tank inventory is dropping in three of the four tanks.
- 12) At approximately 5500 s three of the four tanks had emptied. The fourth tank, which was connected to one of the water/gas nozzles, did not inject any water.

- 13) No action was taken until 6700 s, when water injection from the top was initiated because the melt cooling rate seemed to be limited by the lack of water from the fourth tank.
- 14) Top injection was repeated three more times before the end of the test.
- 15) The thermocouples for the north melt (water nozzles, both tanks functioned) reached saturation temperature at ~6500 s. The thermocouples for the south melt (water/gas nozzles, one tank functioned) reached saturation temperature at ~9000 s.
- 16) The test was terminated at 9065 s.

5. Sensor Malfunctions and Abnormalities

Post test examination of the test apparatus and a preliminary review of the data indicate the following:

- 1) Water was injected from only three of the four reservoirs. However, the injection rate from each of the three that functioned was ~4.5 g/s, close to the target rate of 5 g/s.
- 2) Two of the emptied reservoirs were connected to water nozzles on the north partition, which cooled to saturation temperature first at ~6500 s. One of the two tanks connected to the water/gas nozzles and the south partition did not drain. The south partition did not reach saturation temperature until ~9000 s.
- 3) Both sparge lines began to inject gas at 74 s, but line 2 spiked at around 180 s and then fell to zero at around 280 s. Flow through line 1 was roughly 0.02 lpm for the first 5000 s. Neither of the lines reached the target flow rate of 0.06 lpm,
- 4) The procedure called for water injection from the top shortly after injection from the bottom was observed. This was intended to suppress the temperature of superheated steam early in the transient and avoid damage to the pressure vessel. This early injection was not performed because the upper plenum gas temperature fell quickly to ~700°C, which does not endanger the vessel. Instead, water was added from the top only late in the transient when it appeared that the melt cooling rate might be limited by a lack of water. The cooling rate did indeed rise each time water was injected. There may have yet been water covering the bottom of the melt and the surge in heat flux could have been due to cooling of melt attached to the sides of the liners.
- 5) The flow rate for top injection was measured only for the first injection. The flow rate for each of the three subsequent injections was below the flow meter lower range limit.
- 6) Shortly after the thermite burn was completed and before the isolation valves to the injection lines were opened, some bright flashes were observed in two water hoses indicating some sort of flow through the nozzles and out of the vessel. Figures 5.1 and 5.2 are frames taken from surveillance video. The first figure is a “before” photo with no visible abnormalities while the second figure shows sparks traveling down through the translucent injection line tubing. These flashes were observed for both lines connected to the north partition. Nothing was observed in the lines connected to the south partition. The lines were inspected after the test and there was no evidence of melting or any sort of damage to the tubing. Also, no foreign matter was found within the lines. It is believed that the flashes were caused by a few small and hot particles pushed down the line during the initial pressure spike of thermite ignition and that they had no influence on the course of test.

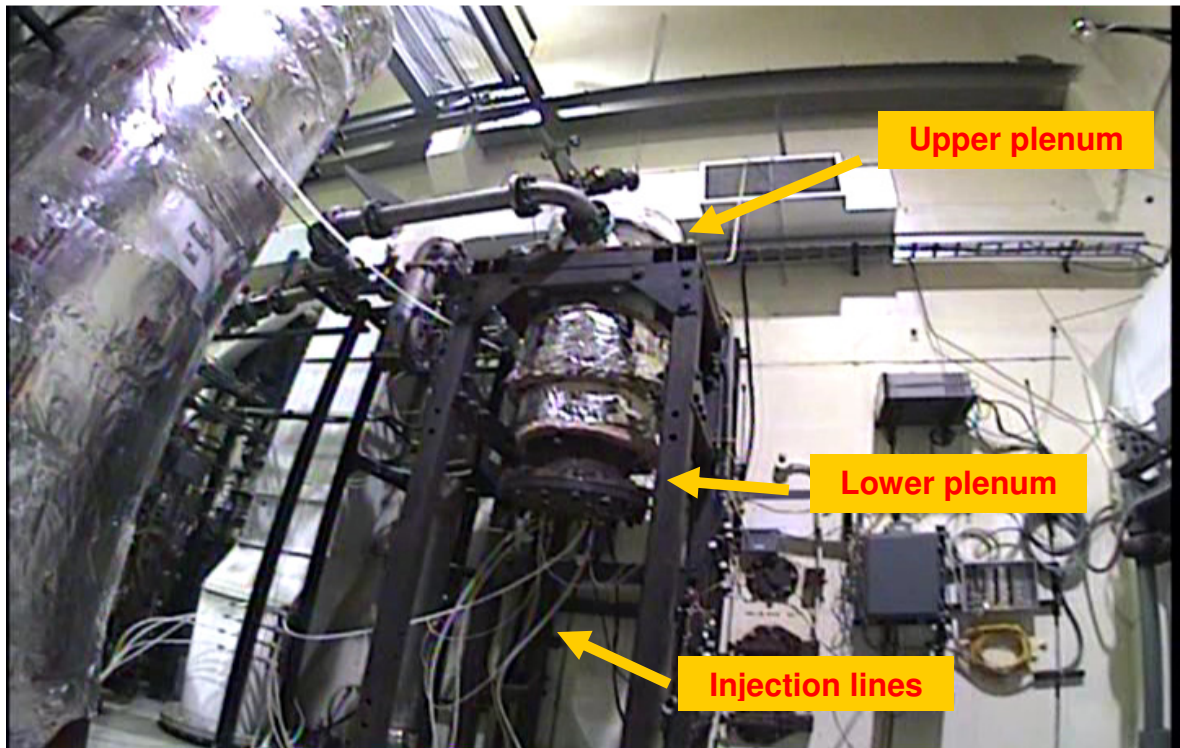


Figure 5.1. SSWICS system shortly after thermite ignition and before an observed anomaly within the translucent tubing of the water injection lines.

Figure 5.2. Bright flashes traveling downward through the reservoir 2 line to the north melt partition. North is to the right of the photo.

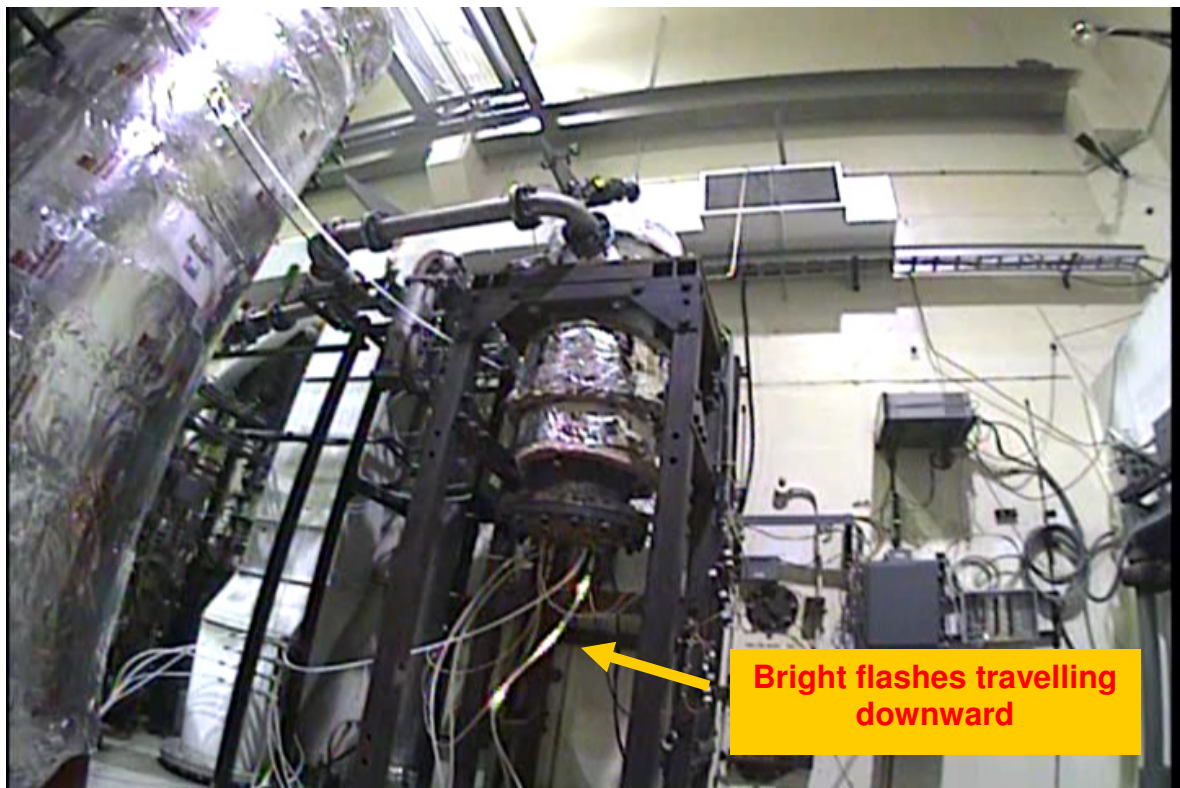


Table 4.2 Test specifications for completed SSWICS experiments.

Parameter	Test Number												
	1	2	3	4	5	6	7	8	9	10	11	12	13
Melt composition (wt% UO ₂ /ZrO ₂ /Cr/ Concrete)	61/25/6/8	61/25/6/8	61/25/6/8	48/20/9/23	56/23/7/14	56/23/6/14	64/26/6/4	56/23/6/14	56/23/6/14	61/25/6/8	56/23/6/14	56/23/6/14	56/23/6/14
Concrete type	LCS	SIL	LCS	LCS	LCS	SIL	LCS	SIL	SIL	SIL	SIL	SIL	SIL
Melt mass (kg)	75	75	75	60	68	68	80	68	23	25	68	136	136
Melt depth (cm)	15	15	15	15	15	15	15	15	5	5	15	30	30
Initial Melt Temperature (°C)	~2300	~2100	~2100	~2100	~2100	~1950	~2100	~1900	-	-	~1850	~2000	~2000
System pressure (bar)	1	1	4	4	4	1	4	1	1	1	1	1	1
Water injection flowrate (lpm)	4	4	12	13	6	14	13	10	9	9	-	-	-
Water injected (liters)	33	39	34	40	61	47	40	41	20	29	>30	~100	~70
Test date (day/mo/year)	30/08/02	17/09/02	30/01/03	13/03/03	15/10/03	24/02/04	14/12/04	25/01/07	14/02/08	5/03/08	05/11/08	09/04/09	12/11/09

6. Data Reduction

Some simple calculations have been performed to provide a preliminary assessment of the test data. The first is a calculation of the coolant inventory in the RV as a function of time. The inventory is the difference between the total amount of liquid injected and the amount boiled off and collected in the CT:

$$M_{H_2O-RV} = \sum_{t=0}^{t=t_{end}} \rho \dot{V} \Delta t - \frac{\pi D^2}{4} \frac{\Delta P}{g} \quad (6.1)$$

where data from sensor F-quench is used for the volumetric flow rate \dot{V} and the liquid density ρ is taken to be 998 kg/m³. The condensate inventory is calculated with readings from sensor PD-CT (ΔP) and the tank diameter D of 0.203 m.

The corium heat flux was calculated using two different methods. The first considers the rate of condensate collection, which is a measure of the steam flow rate from the RV. Accurate determination of the heat flux at the corium surface must, however, account for various heat sinks. During the injection phase, energy is absorbed raising the coolant to the saturation temperature. Some of the vapor produced by the quenching melt condenses on the walls of the upper plenum to heat the RV structures to the saturation temperature. Later, heat losses from the upper plenum generate continued condensation. Accounting for these heat sinks, the rate of energy transfer through the corium surface is written as:

$$Q = M_{RV} c_p \frac{\partial T}{\partial t} + \dot{m} h_{fg} + [M_s c_M \frac{\partial T}{\partial t} + Q_{HL}] \Big|_{up} \quad (6.2)$$

where \dot{m} is mass flow rate of condensate into the CT, M_s is the mass of the RV upper plenum structures, c_M is their heat capacity, and Q_{HL} represents total upper plenum heat losses. For this report, liquid subcooling has been neglected (an accurate assumption after the injection phase) along with heat losses and time variations in structure temperatures. The condensation rate is calculated from the time derivative of the differential pressure signal PD-CT. The heat transfer rate from the corium is then:

$$Q = \frac{1}{g} \frac{\pi}{4} D^2 \frac{\partial \Delta P}{\partial t} h_{fg} \quad (6.3)$$

where D is again the inner diameter of the CT and the heat of vaporization h_{fg} is 2256 kJ/kg°C (TG-RV registered 100°C through most of the transient). The heat flux is obtained by scaling Q with the initial surface area of the corium (0.071 m²). The derivative was calculated with pairs of averaged ΔP readings (an average of 5 measurements at 0.5 Hz) centered around a Δt of 60 s. The averaging and length of Δt were necessary to reduce oscillations in the calculated heat flux.

The second method of calculating corium heat flux uses an energy balance on the secondary side of the heat exchanger. The measured parameters are the coolant flow rate on the secondary side of the cooling coils and the inlet and outlet coolant temperatures. The cooling power of the heat exchanger is then:

$$Q_{HX} = \rho \dot{V}_{HX} c_p (T_{out} - T_{in}) \quad (6.4)$$

where readings from sensors TF-HX-in and TF-HX-out were used for temperatures T_{in} , and T_{out} , respectively. Data from the flow meter F-HX was used for \dot{V}_{HX} while the density and heat capacity of water were taken to be 982 kg/m³ and 4.18 kJ/kg°C, respectively.

The cooling power of the heat exchanger is related to the steam flow rate out of the RV by the following:

$$Q_{HX} = \dot{m} [h_{fg} + c_p (T_{sat} - T_{con})] \quad (6.5)$$

where \dot{m} is the mass flow rate of steam into the heat exchanger (identical to the flow rate of condensate into the CT, as defined in equation 5.2). From equation 6.5 it can be seen that if condensate leaves the heat exchanger at the saturation temperature, i.e., there is no subcooling, the cooling power of the heat exchanger is equal to the product of \dot{m} and h_{fg} . In this case, according to equation 6.2, the cooling power of the heat exchanger equals the heat transfer rate from the melt. However, the condensate does not, in general, leave the heat exchanger at the saturation temperature. The result of this subcooling is an overestimation of the corium heat flux when using equation 6.5 and the assumption of $T_{sat} = T_{con}$.

The corium heat flux could be calculated more accurately with the heat exchanger energy balance through the addition of a condensate temperature measurement at the heat exchanger outlet. However, the calculation would still require the steam mass flow rate, which would be derived from the CT level measurements. Thus the heat exchanger energy balance, with the assumption of $T_{sat} = T_{con}$, is considered to be a rough check of the heat flux measurements derived directly from the CT level measurements using equation 6.3.

Note: the heat flux estimate described above assumes a well-defined corium surface area. In early tests, nearly all the corium remained within the bottom liner to form an ingot with a surface area defined by the inner diameter of the MgO liner. However, Tests 12 and 13, with water injection from the bottom, have ejected melt throughout much of the test section and so corium surface area is not well defined. The heat flux plot in Fig. A.12 is useful mainly for comparing the heat load with previous tests. This could also be done without assumptions of corium geometry by comparing condenser heat loads in Watts. Previous test results were presented in terms of heat flux due to our interest in measuring the dryout heat flux and so results are shown here with the same scaling even though the corium surface area is not well defined, at least in the early part of the test when the relatively thin layer of material covering the upper surfaces is quenched to T_{sat} .

7. Post Test Exams

Disassembly of the pressure vessel indicated that melt was ejected upwards in a fashion similar to that of the previous test. However, there was much less corium in the upper liners and none on the lid. The stainless steel liner was coated with a rather even layer of corium with a thickness of 1-2 mm. It was not possible to weigh this corium separately because it was not firmly attached to the steel and much of it fell into the lower plenum with other debris during disassembly.

Figure 7.9 shows the distribution of corium collected from the vessel. As the apparatus was disassembled, corium was collected and weighed. The top zone consists of the steel liner and the second zone corresponds to the top MgO liner. The third encompasses the entire lower plenum. The amount of corium attached to the liner is, based on the observed thickness range and a density of 6000 kg/m³, estimated to be between 1.7 and 3.4 kg. Corium was firmly attached to the MgO liners and so the mass in the second zone could be determined directly by chipping corium away from liner and weighing it separately. Corium from this second zone weighed 9.5 kg. Corium that fell from the steel liner was combined with loose debris taken out of the lower plenum. This was weighed and found to be 11.5 kg. The remaining corium was firmly affixed to the liners of the lower plenum and the tungsten plates. This material is estimated to be 113 kg based on the initial charge of 136 kg.



Figure 7.1. Top view of MgO basemat showing nozzles and thermowells.

Figure 7.2 Basemat after addition of concrete layer.

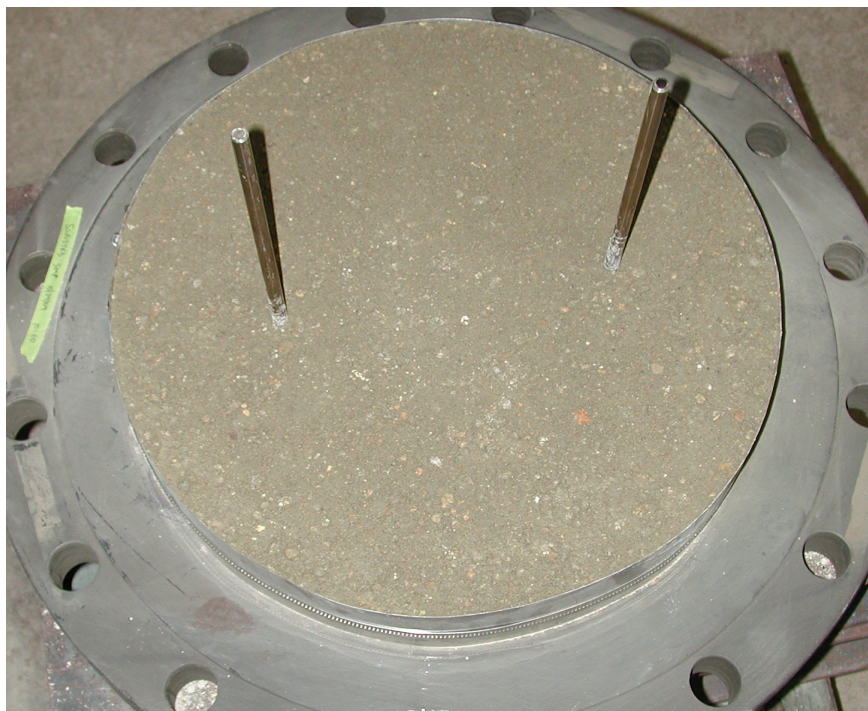




Figure 7.3. Lower plenum assembly with MgO liners on basemat.

Figure 7.4. Top view of lower plenum assembly before loading corium.





Figure 7.5. Lower plenum post test.

Figure 7.6. South partition after removal of loose debris.





Figure 7.7. North partition after removal of loose debris.

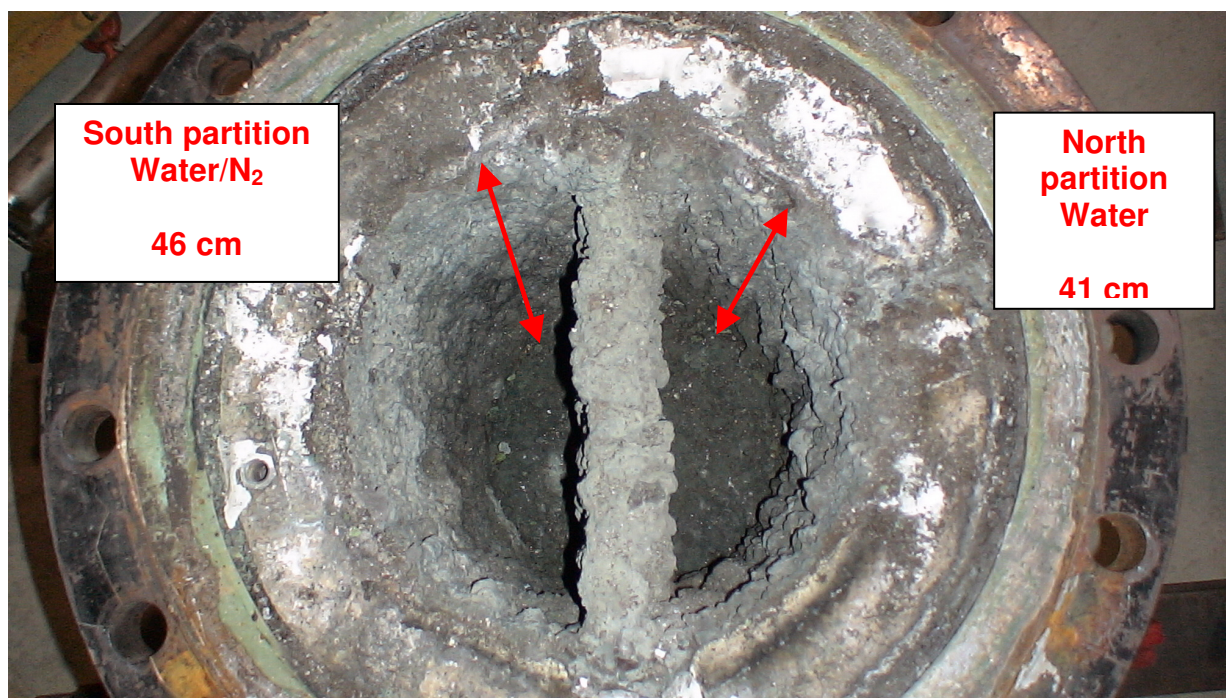


Figure 7.8. Corium levels in each partition after removal of loose debris. The level was measured from corium surface to top of MgO liner, which is 62 cm above the nozzle outlets. Corium depths are therefore approximately: north 21 cm and south 16 cm.

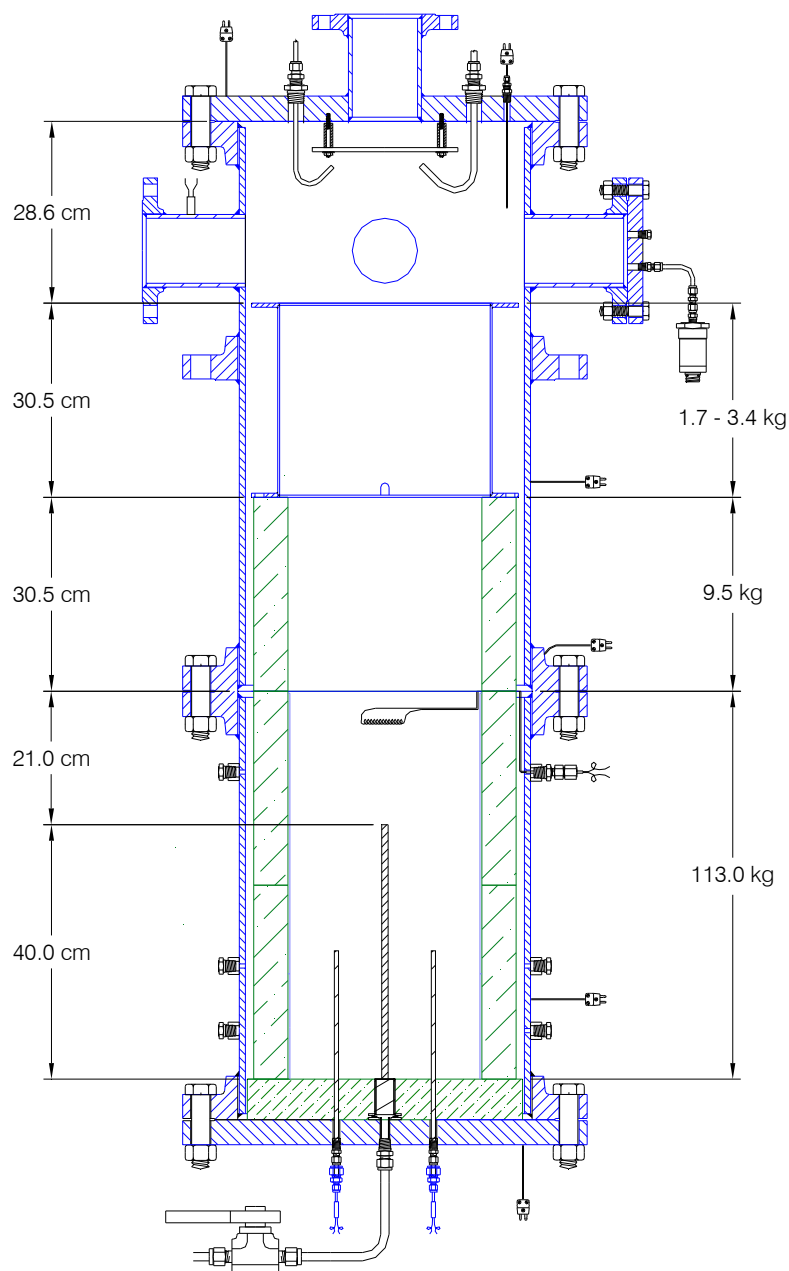


Figure 7.9. Posttest corium distribution. The weight of crust attached to the steel liner was calculated using the observed thickness of 1-2 mm. Crust attached to the top MgO liner was chipped away and weighed. Loose material from various regions weighed 11.5 kg. The balance in the lower 61 cm, based on the initial 136 kg thermite charge, is ~113 kg.

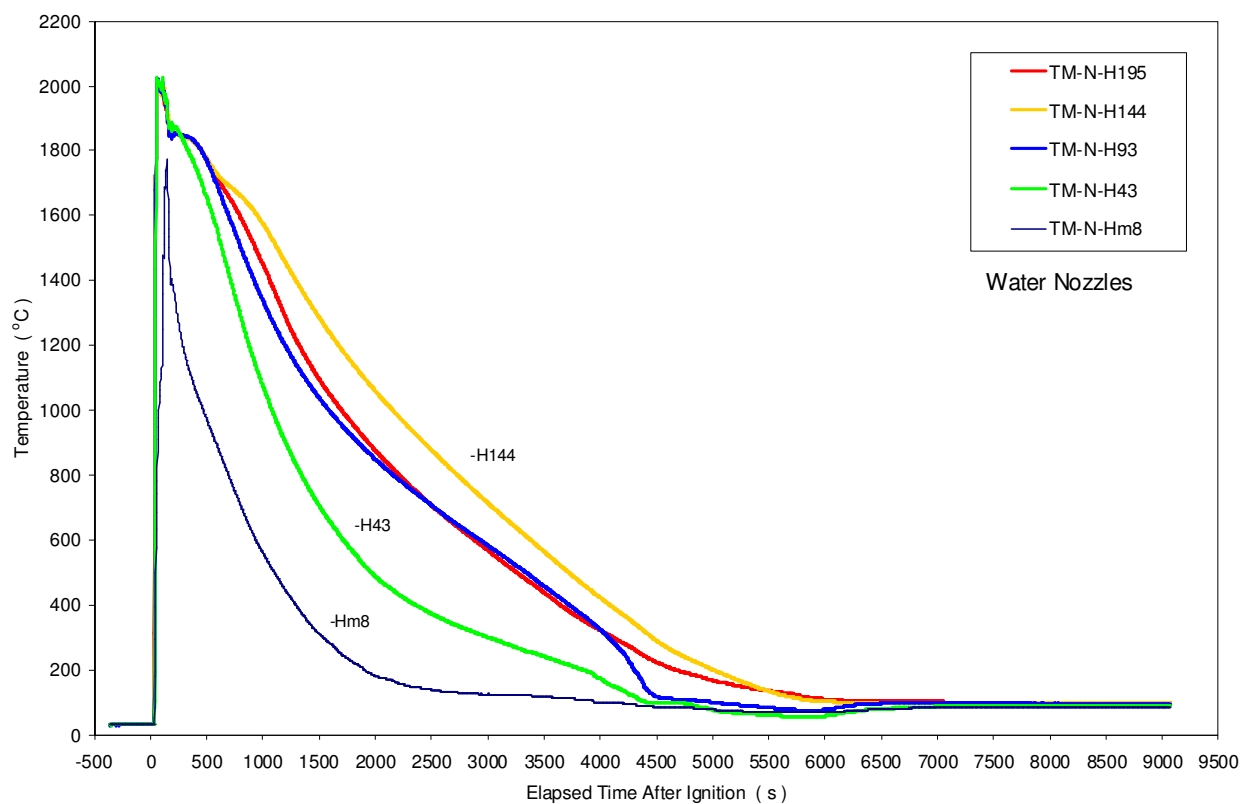
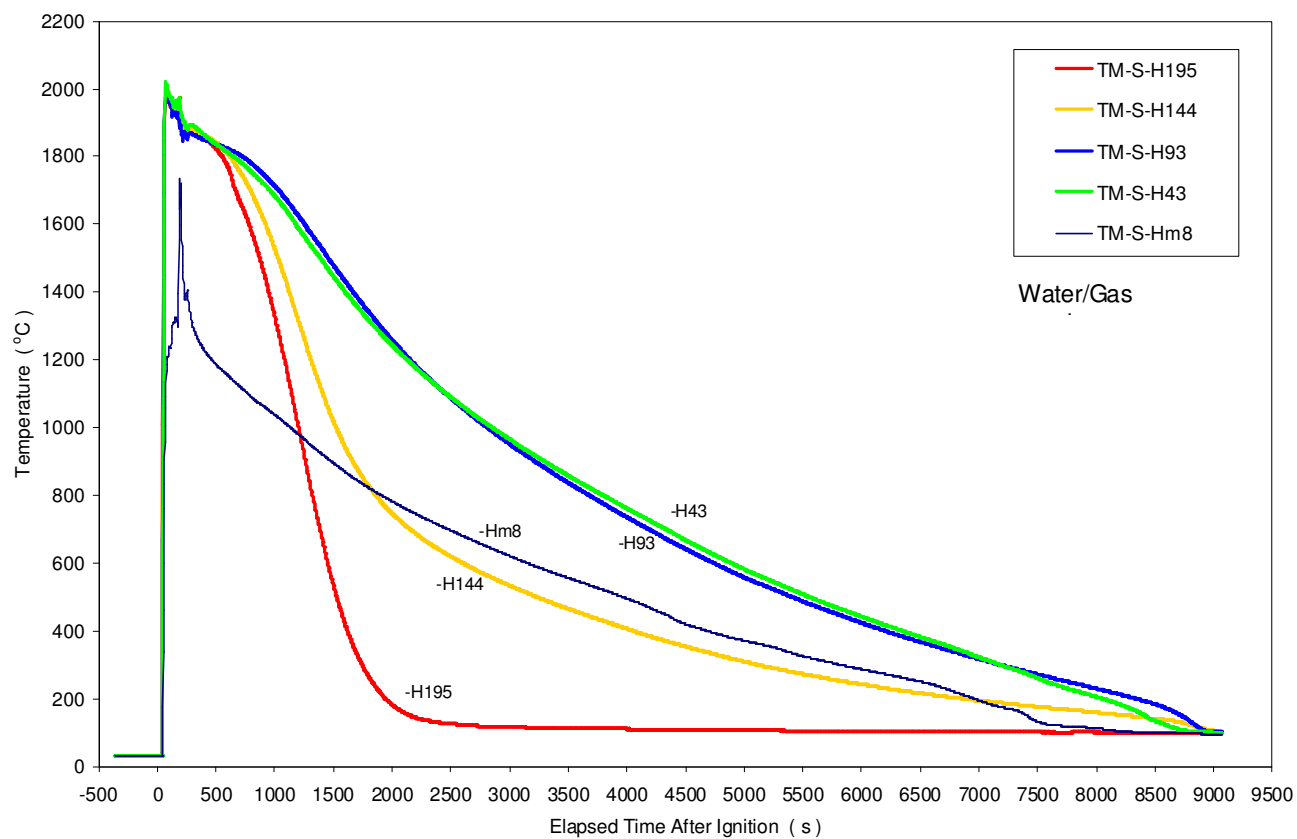


Figure A.1 Temperatures in tungsten thermowell; north melt quadrant.

Figure A.2 Temperatures in tungsten thermowell; south melt quadrant.



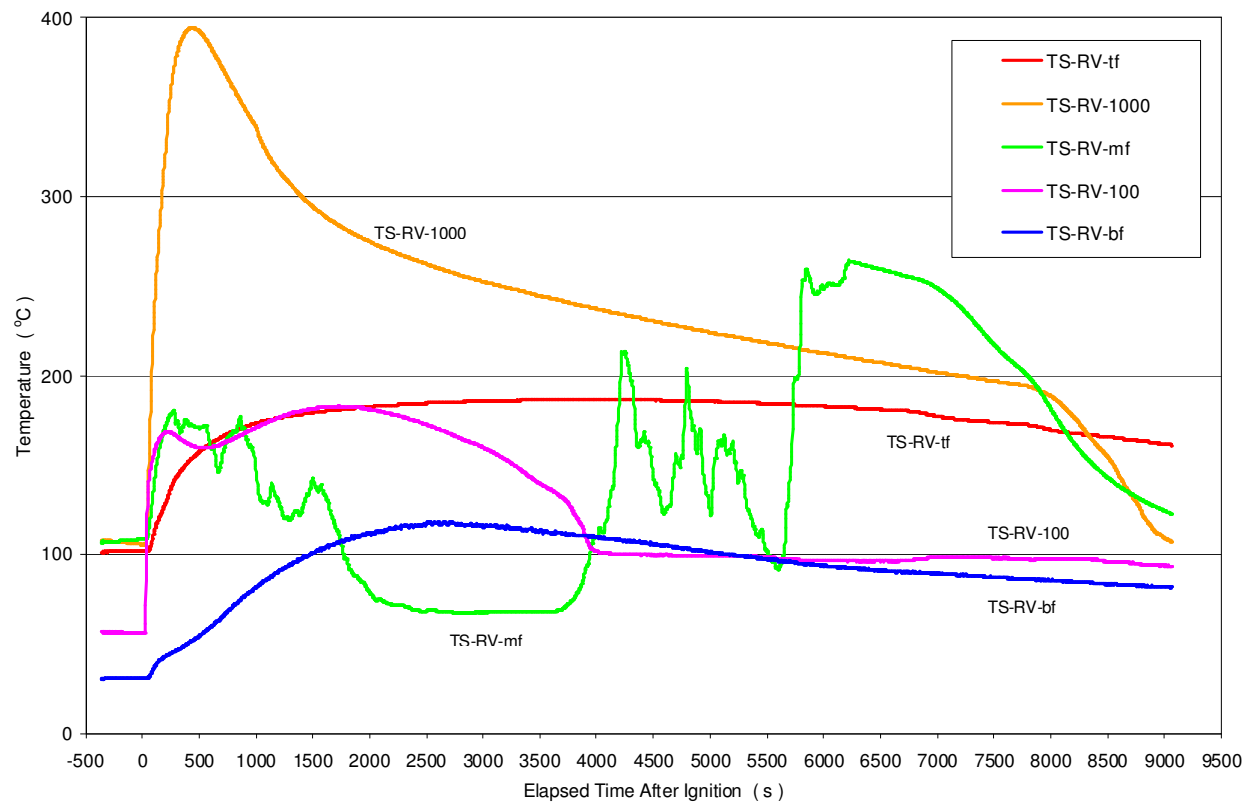
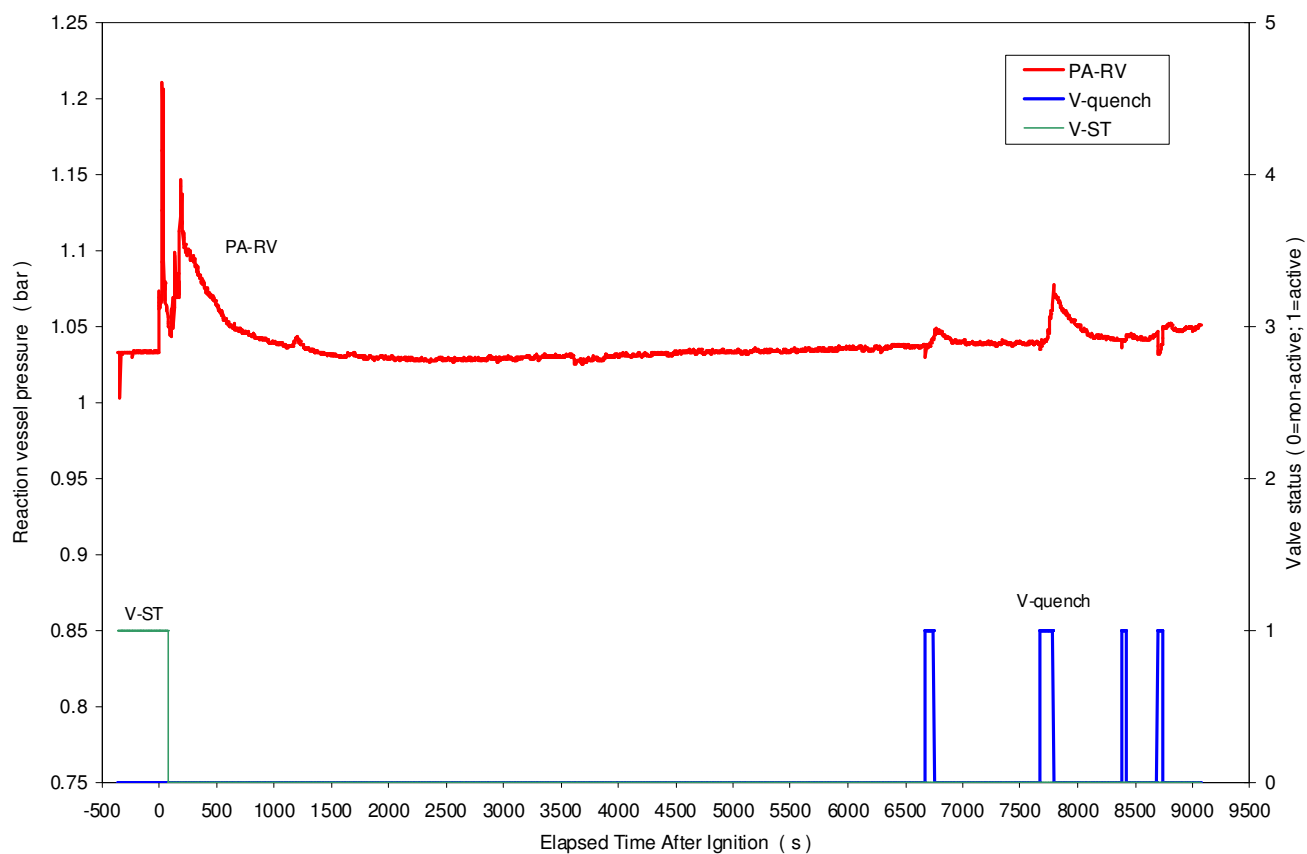


Figure A.3 Temperatures of selected steel structures.

Figure A.4 Total pressure in reaction vessel and positions of selected valves.



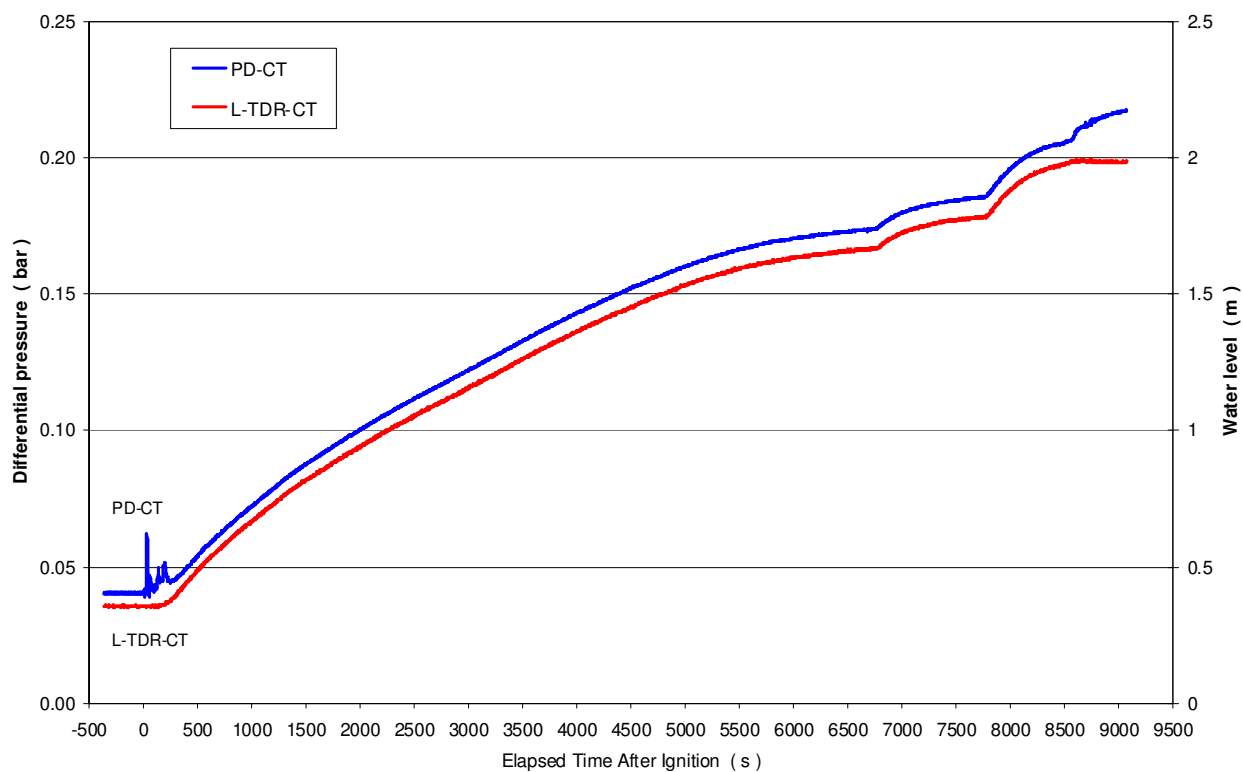
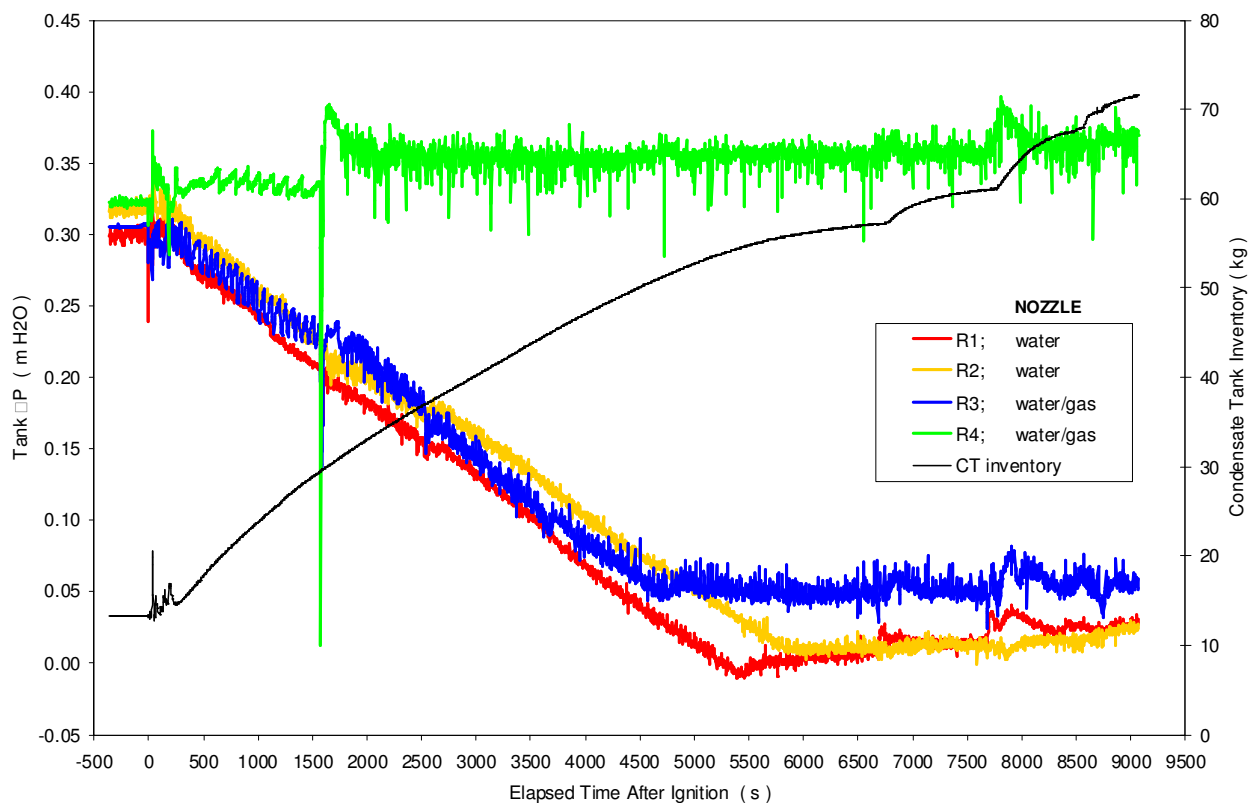


Figure A.5 Condensate tank inventory as measured by ΔP and level sensors.
Figure A.6 Reservoir levels and condensate tank liquid inventory.



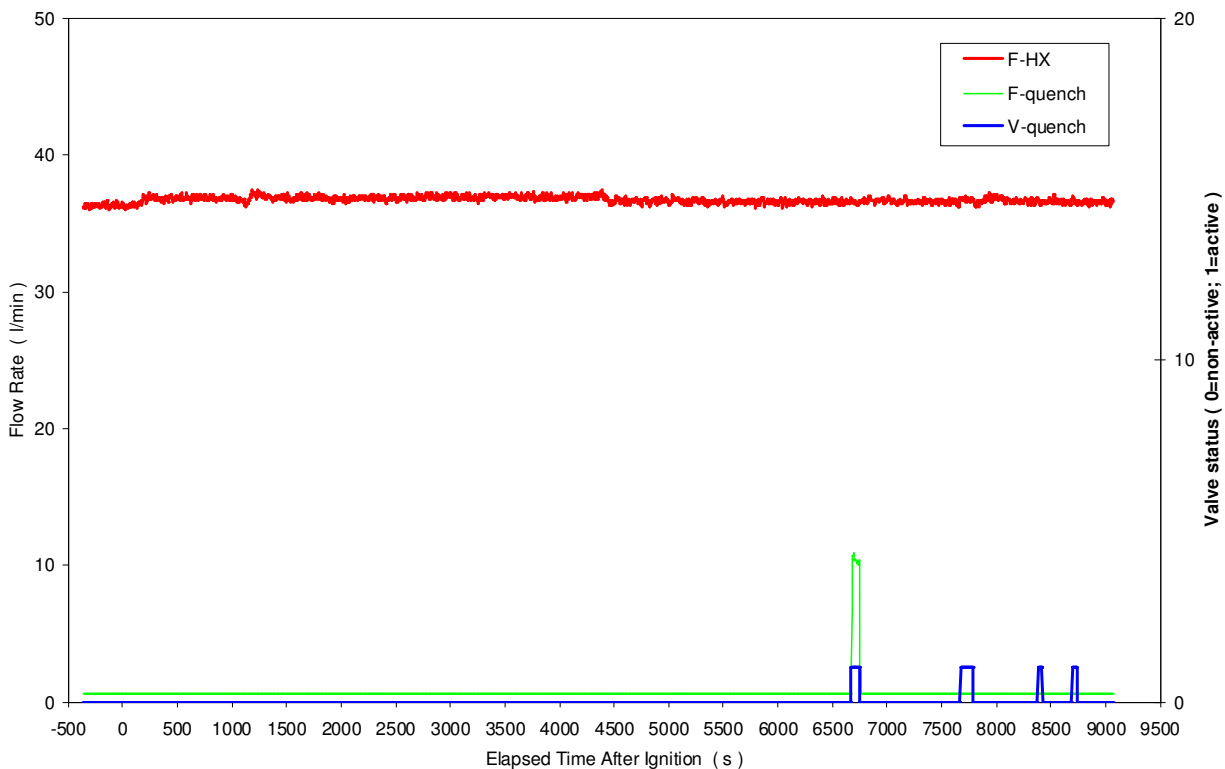
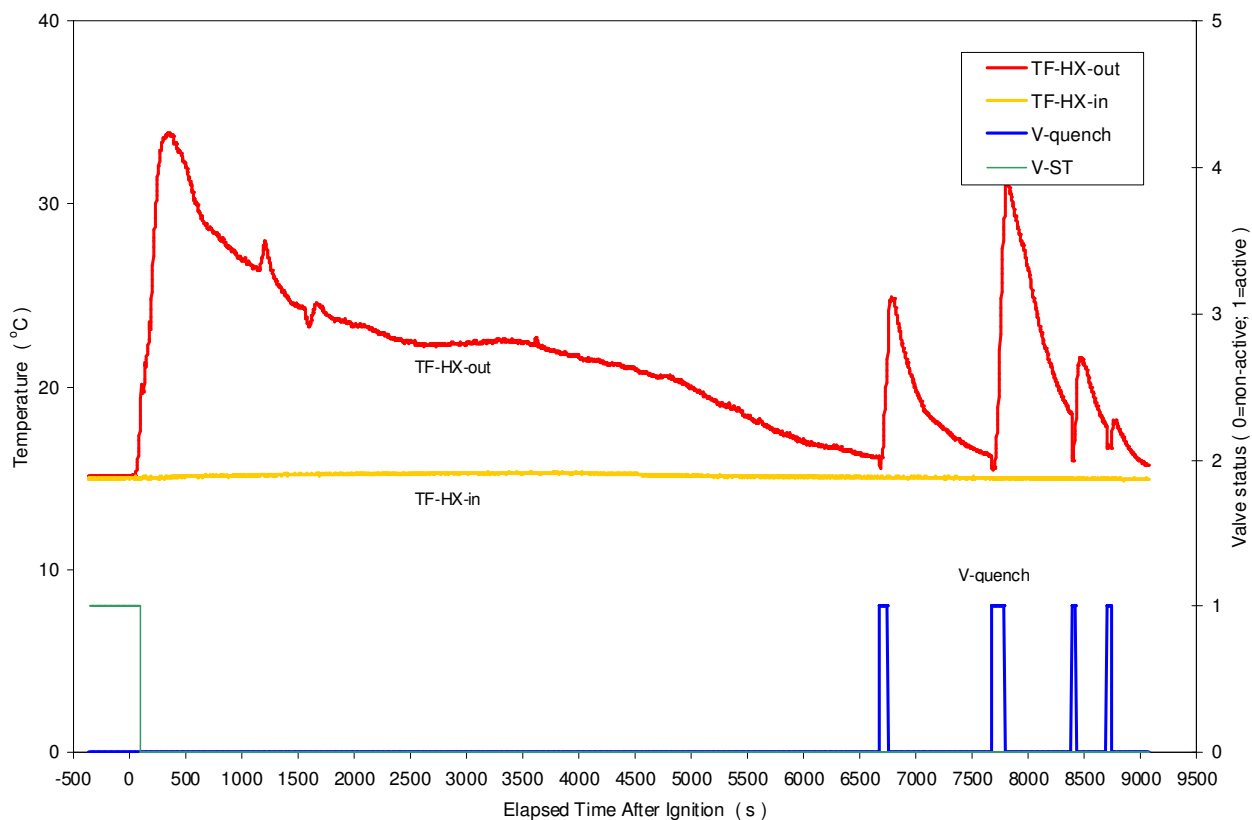


Figure A.7 HX secondary side flow rate, injection flow rate, and water injection valve position.
Figure A.8 Secondary side fluid temperatures at HX inlet and outlet.



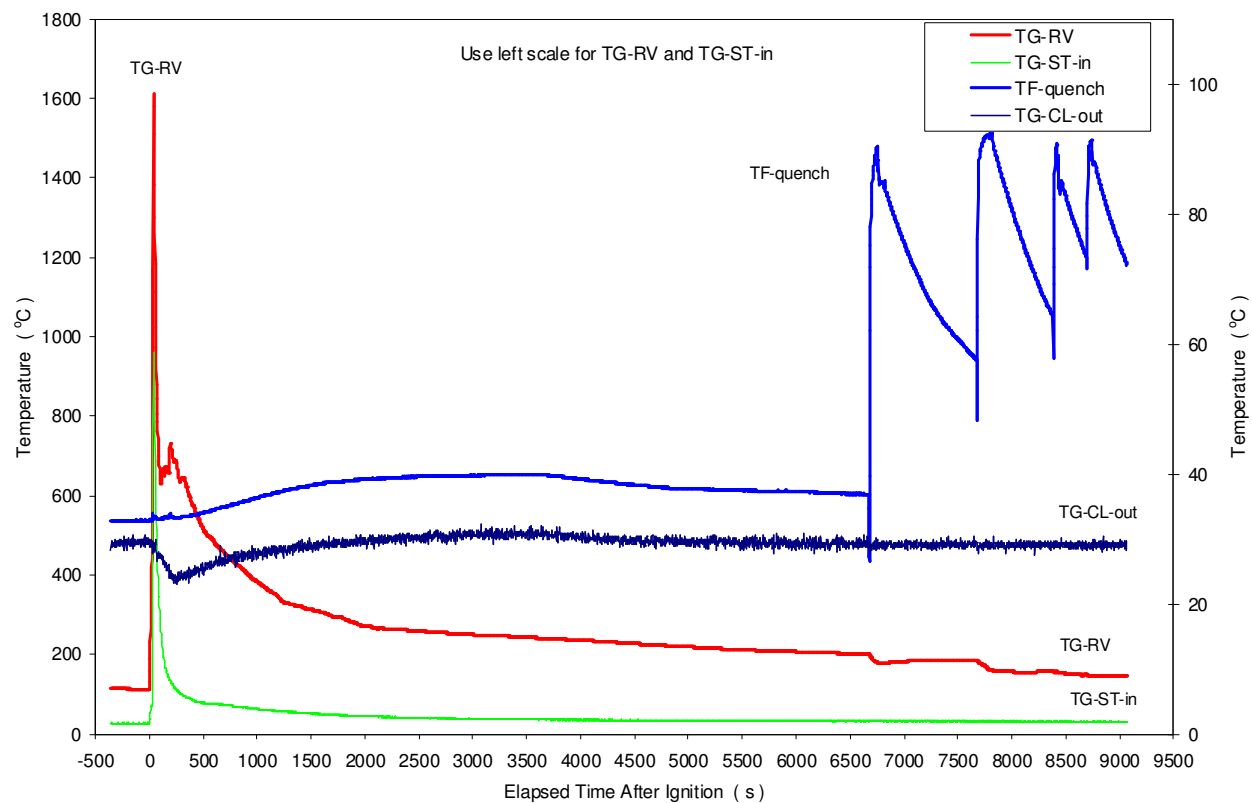
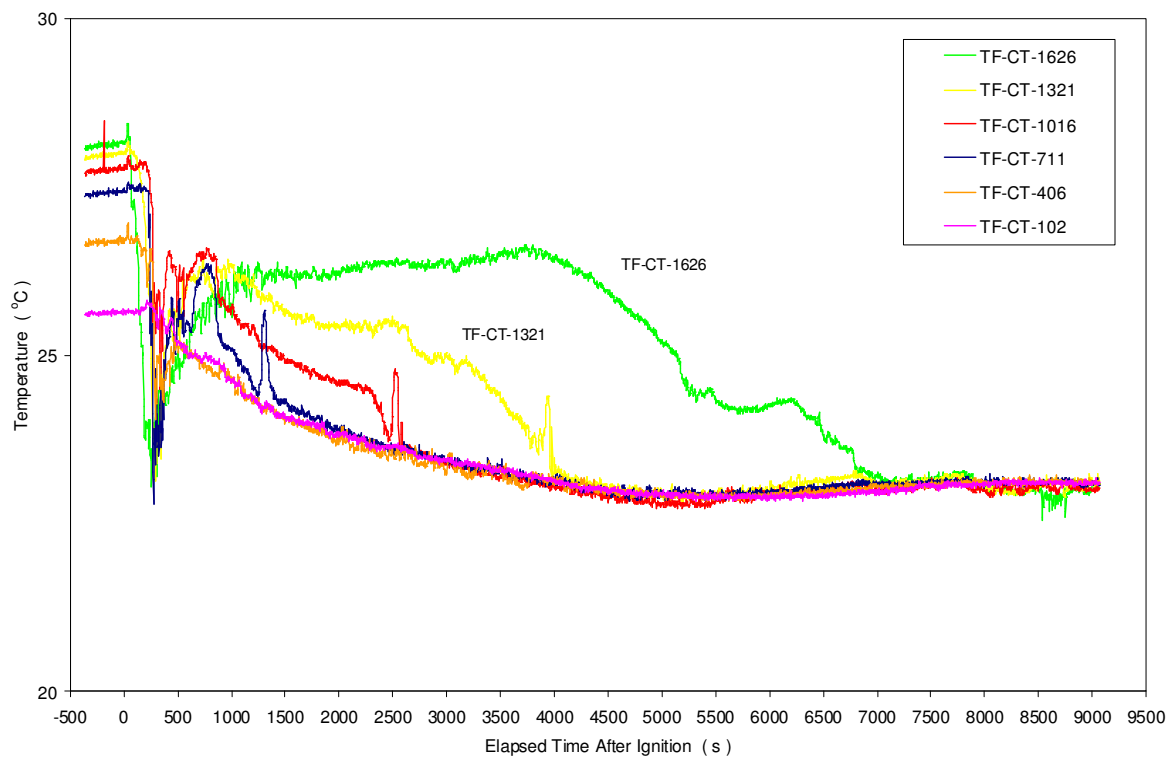


Figure A.9 Miscellaneous gas and fluid temperatures.
Figure A.10 Fluid temperatures in the condensate tank.



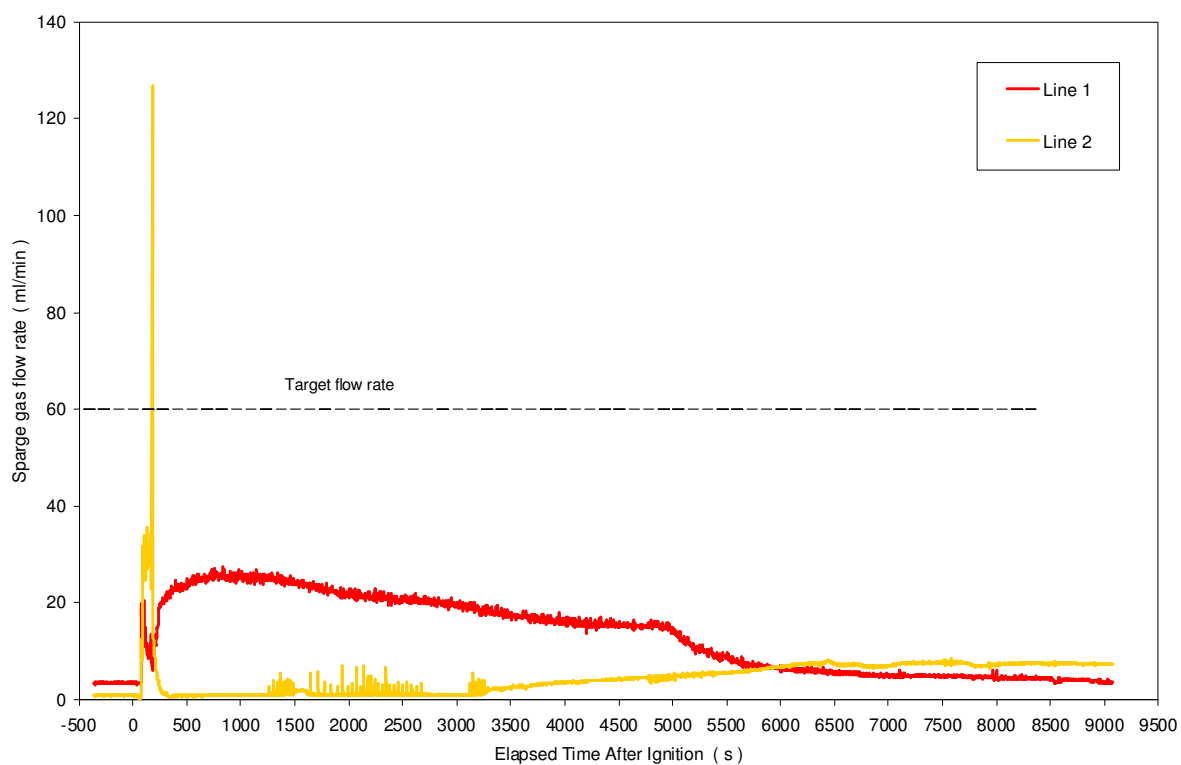


Figure A.11 Sparge gas (N₂) flow rates.

Figure A.12 Heat flux as measured through condensate tank levels and HX heat load. See note at end of section 6.

